Molecular Therapy
Original Article

Transient secretion of VEGF protein from transplanted hiPSC-CMs enhances engraftment and improves rat heart function post MI

Xuefeng Ai,[1,7] Bingqian Yan,[2,7] Nevin Witman,[3,4] Yiqi Gong,[1] Li Yang,[5] Yao Tan,[2] Ying Chen,[2] Minglu Liu,[1] Tingting Lu,[2] Runjiao Luo,[1] Huijing Wang,[2] Kenneth R. Chien,[3] Wei Wang,[1] and Wei Fu[2,6]

[1]Department of Pediatric Cardiothoracic Surgery, Shanghai Children's Medical Center, School of Medicine, Shanghai Jiao Tong University, Shanghai 200127, China; [2]Institute of Pediatric Translational Medicine, Shanghai Children's Medical Center, School of Medicine, Shanghai Jiao Tong University, Shanghai 200127, China; [3]Department of Cell and Molecular Biology, Karolinska Institutet, 17165 Stockholm, Sweden; [4]Department of Clinical Neuroscience, Karolinska Institutet, 17177 Stockholm, Sweden; [5]Department of Anesthesiology, Fudan University Shanghai Cancer Center; Department of Oncology, Shanghai Medical College, Fudan University, Shanghai 200032, China; [6]Shanghai Key Laboratory of Tissue Engineering, Shanghai 9th People's Hospital, School of Medicine, Shanghai Jiao Tong University, Shanghai 200011, China

Cell-based therapies offer an exciting and novel treatment for heart repair following myocardial infarction (MI). However, these therapies often suffer from poor cell viability and engraftment rates, which involve many factors, including the hypoxic conditions of the infarct environment. Meanwhile, vascular endothelial growth factor (VEGF) has previously been employed as a therapeutic agent to limit myocardial damage and simultaneously induce neovascularization. This study took an approach to transiently overexpress VEGF protein, in a controlled manner, by transfecting human induced pluripotent stem cell-derived cardiomyocytes (iPSC-CMs) with VEGF mRNA prior to transplantation. The conditioning of iPSC-CMs with VEGF mRNA ultimately led to greater survival rates of the transplanted cells, which promoted a stable vascular network in the grafted region. Furthermore, bulk RNA transcriptomics data and Kyoto Encyclopedia of Genes and Genomes (KEGG) pathway analysis revealed that phosphoinositide 3-kinase (PI3K)-protein kinase B (Akt) and AGE-RAGE signaling pathways were significantly upregulated in the VEGF-treated iPSC-CMs group. The over-expression of VEGF from iPSC-CMs stimulated cell proliferation and partially attenuated the hypoxic environment in the infarcted area, resulting in reduced ventricular remodeling. This study provides a valuable solution for the survival of transplanted cells in tissue-engineered heart regeneration and may further promote the application of modified mRNA (modRNA) in the field of tissue engineering.

INTRODUCTION

Heart failure (HF) stemming from ischemic events is a leading cause of global morbidity, and the clinical treatments for patients with a poor prognosis are extremely limited.[1] Cell-based therapies are proving to be a potential, prominent, and novel treatment option for HF patients. Current pre-clinical and clinical studies have employed skeletal muscle myoblasts (SMs),[2] mesenchymal stem cells (MSCs),[3-5] bone marrow mononuclear cells (BMMNCs),[6-8] endothelial progenitor cells (EPCs),[9] and human induced pluripotent stem cell (iPSC)-derived cardiomyocytes (CMs)[10-12] to repair damaged myocardial tissue and enhance global cardiac function. The major mechanisms of action reported by these cell therapies are to either stimulate cardiac repair processes through the release of soluble factors or via engraftment with the host myocardium, which partially restores the pumping capacity of the heart muscle.[13-15] Several major caveats continue to limit the use of cell-based therapies for heart repair, including the limited survival and death of the transplanted cells.[10,16,17] Improving the survival rates of transplanted cells could lead to substantially better outcomes.

In order to overcome the limitations of poor transplantation efficiency and survival, cells have been combined with biomaterials such as modified hydrogels,[18,19] engineered heart tissue (EHT) constructs,[20] and engineered heart muscle (EHM).[21] Additional efforts to improve cell survival have focused on modulating the levels of inflammation in the injury site by targeting inflammatory cytokines or reactive oxygen species.[22,23] Alternative methods for improving cell viability and grafting efficiency include genetic engineering approaches (such as using lentivirus to genetically enhance the seed cells),[12] or pre-conditioning the seed cells with cytokines or drug

Received 9 March 2022; accepted 12 August 2022;
https://doi.org/10.1016/j.ymthe.2022.08.012.

[7]These authors contributed equally

Correspondence: Department of Pediatric Cardiothoracic Surgery, Shanghai Children's Medical Center, School of Medicine, Shanghai Jiao Tong University, Shanghai 200127, China.
E-mail: wangwei@scmc.com.cn
Correspondence: Institute of Pediatric Translational Medicine, Shanghai Children's Medical Center, School of Medicine, Shanghai Jiao Tong University, Shanghai 200127, China.
E-mail: fuweizhulu@163.com

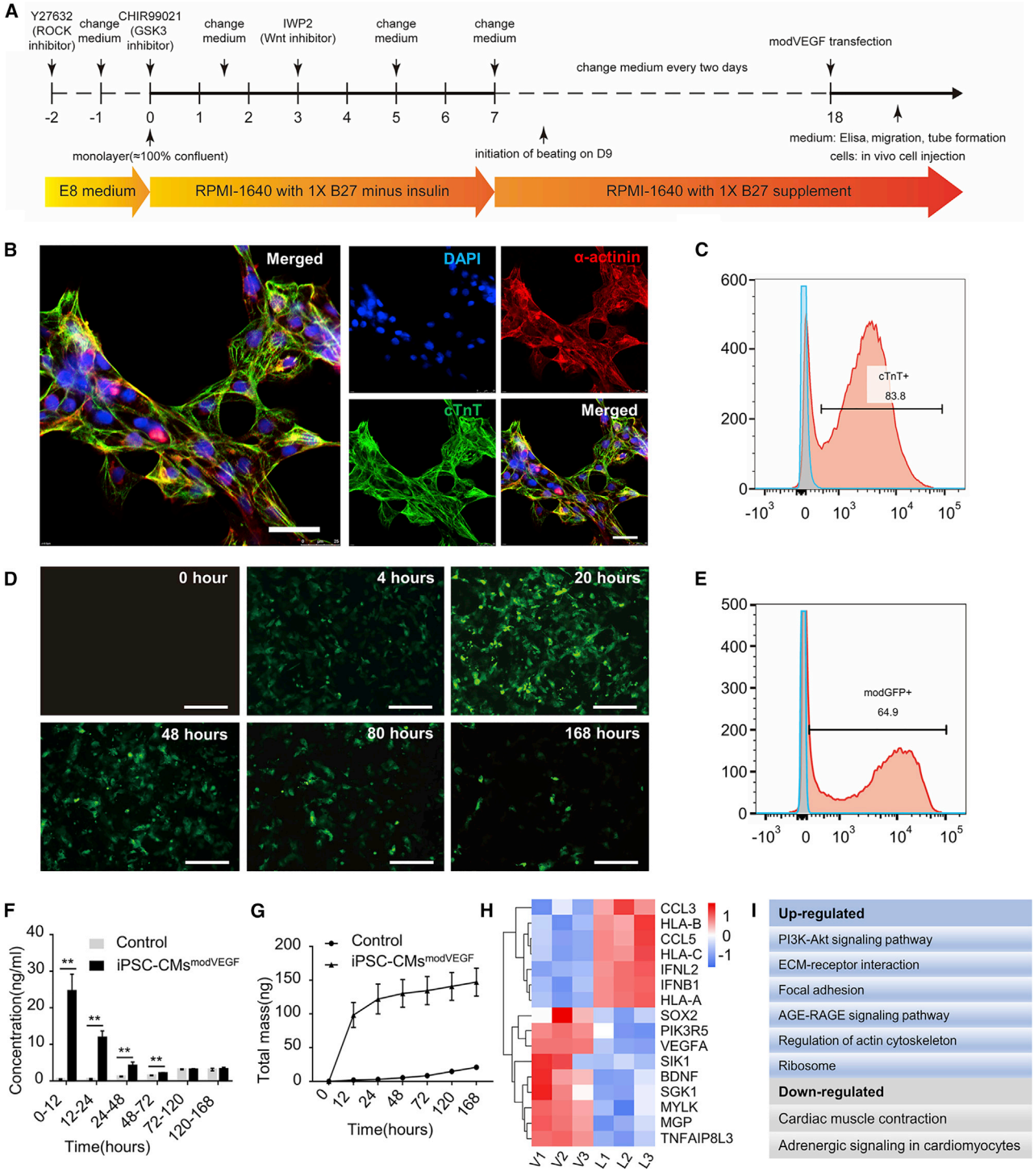

Figure 1. Cardiac differentiation and characteristics of iPSC-CMs following modRNA transfection

(A) Schematic diagram of the protocol for CM differentiation from iPSCs. (B) Representative immunostaining images of CMs on day 18 of differentiation with myocardial structural markers cTnT, α-actinin. Scale bar, 25 μm. (C) Cardiac troponin expression on day 18 was analyzed by flow cytometry (n = 3). (D–G) Transfection efficiency and secretion kinetics of VEGF modRNA in iPSC-CMs. (D) Representative photomicrographs of CMs at 0, 4, 20, 48, 80, and 168 h post transfection with a modGFP reporter. Scale bar, 200 μm. (E) Representative flow cytometry analysis from modGFP-transfected iPSC-CMs at 20 h post transfection. (F and G) Kinetics of (F) newly produced and

(legend continued on next page)

inhibitors to ultimately prohibit activation of pro-apoptotic pathways following transplantation.[24-26]

On the other hand, *in vivo*-produced protein from the delivery of chemically modified mRNAs (modRNAs) have more recently come to light as a novel tool for cardiac therapy. Transiently expressed modRNAs overcome safety concerns that are often met with traditional gene therapies, such as immunogenicity and genetic integration.[27] In 2013, Zangi et al. delivered a single dose of vascular endothelial growth factor (VEGF)-A_{165} modRNA to the infarcted mouse myocardium and reported neo-angiogenesis, enhanced cardiac function, and prolonged survival rates of the mice receiving the treatment.[28] More recently, VEGF-A modRNA was used in a large animal model of HF, where it increased capillary densities, reduced fibrosis, and improved global heart function.[29] Alternative modRNA candidates have emerged for cardiac repair therapy and were reported to stimulate CM proliferation,[30] induce CM cell-cycle events,[31] as well as promote CM cell survival following infarction.[32]

Recent work by our research teams have shown that using cells as a carrier to deliver modRNA can increase the expression efficiency of the target protein *in vivo*, which improves the overall therapeutic effects and allows one to greatly reduce the amount of mRNA needed to generate a physiological response.[33,34] In this paper, we sought to take a combinatorial approach that would unite cell therapy strategies with novel mRNA technologies to better enhance cardiac regeneration. The aim of this work was therefore to investigate the functional efficiency of transiently secreting VEGF from iPSC-CMs for myocardial repair in a rat model of myocardial infarction (MI).

RESULTS

Cardiac differentiation and properties of iPSC-CMs

In this study we hypothesized that iPSC-CMs loaded with VEGF modRNAs could enhance CM graft survival, possibly leading to increased functional restoration following MI injury. As a first step we cultured, expanded, and differentiated iPSCs into beating CMs using previously reported protocols (Figure 1A).[35] Prior to differentiation, identification of the iPSCs stemness was performed by labeling the cells for pluripotency markers: Sox2/Oct4/Nanog/Tra-1-60 (Figures S1A–S1D). CMs cultured to the 18th day were used as seed cells for subsequent *in vitro* and *in vivo* experiments. The iPSC-derived CMs presented a round or polygonal shape and expressed abundant sarcomeric structures and myocardial-specific markers cardiac troponin T (cTnT) and α-actinin (Figure 1B). Cellular changes were recorded during differentiations and transmission electron microscopy confirmed the presence of myofilament fibers, Z lines, mitochondria, and gap junctions within the CMs (Figures S2A and S2B). CMs derived from the iPSCs also showcased typical action potentials (Figure S2C).[36] The efficiency of the CM differentiation protocol was robust, with approximately 83.8% of the cells taking on a CM cell fate (Figure 1C).

Additionally, we performed myosin light chain-2a (MLC2a) and myosin light chain-2v (MLC2v) labeling to identify CM maturation at 18 days post differentiation. Immunofluorescent labeling analysis revealed that 17.7% ± 2.6% of the $cTnT^{+}$ iPSC-CMs exhibited the mature ventricular CM marker MLC2v, whereas 99.3% ± 0.2% of the iPSC-CMs expressed MLC2a, a phenotypic indication of a predominantly immature ventricular CM population (Figures S3A–S3C). When further exploring the length-to-width ratios, the results indicated that 89.2% of CMs presented with a length/width ratio less than 3:1 and only 0.2% of CMs presented with a length/width ratio of more than 7:1 (Figure S3D).[36] These data further confirmed that the majority of iPSC-CMs differentiated to day 18 were of a relatively immature phenotype.

iPSC-CMs tolerate modRNA transfection and exhibit enhanced proangiogenic properties *in vitro*

Next, to verify the efficient uptake and translation of modRNA in iPSC-CMs, we first transfected the cells with a green-fluorescent protein (GFP) reporter construct. We observed that the iPSC-CMs began to express GFP protein at 4 h post transfection and the signal intensity peaked by 20 h post transfection (Figure 1D). Flow cytometry analysis found that the transfection of modRNA into iPSC-CMs was highly efficient at 20 h post transfection (64.9%), but the GFP protein signal gradually tapered off over the course of 7 days post transfection (Figures 1D and 1E). Noticeably, Calcein-AM/propidium iodide (PI) staining revealed that modRNA transfections had no significant effect on cell viability (Figures S4A–S4C). Importantly, the iPSC-CMs retained their synchronous beating potential following the transfection of the modRNAs, indicating limited cytotoxicity of the procedures, which can be seen in the supplemental data (Figure SV1).

To determine the forced secretion kinetics of modRNA-transfected iPSC-CMs, we over-expressed the cells with mRNA transcripts encoding the VEGF-A_{165} gene. Levels of newly produced and accumulating VEGF protein were assessed and compared between the iPSC-CMs transfected with VEGF modRNA (iPSC-$CMs^{modVEGF}$) and the untransfected iPSC-CMs. The *de novo* VEGF protein secretion levels were significantly higher in the iPSC-$CMs^{modVEGF}$ group compared with the untransfected group for the first 3 days (Figure 1F). When investigating the magnitude of cumulative VEGF protein, the levels found in the iPSC-$CMs^{modVEGF}$ group were significantly higher compared with the untransfected group at all time points evaluated (Figure 1G).

(G) cumulative VEGF protein concentration at denoted time points after transfection of modVEGF into iPSC-CMs. p values were determined by one-way analyses of variance followed by Bonferroni post test. *$p < 0.05$, **$p < 0.01$. (H) Heatmap of differentially expressed genes (DEGs) related to growth and metabolism of iPSC-CMs; each rectangle represents one gene, blue indicates low-intensity expression, red indicates high-intensity expression. (I) KEGG pathway analysis reveals the most up/downregulated pathways (related to cell growth and metabolism), as a result to VEGF mRNA transfection in iPSC-CMs.

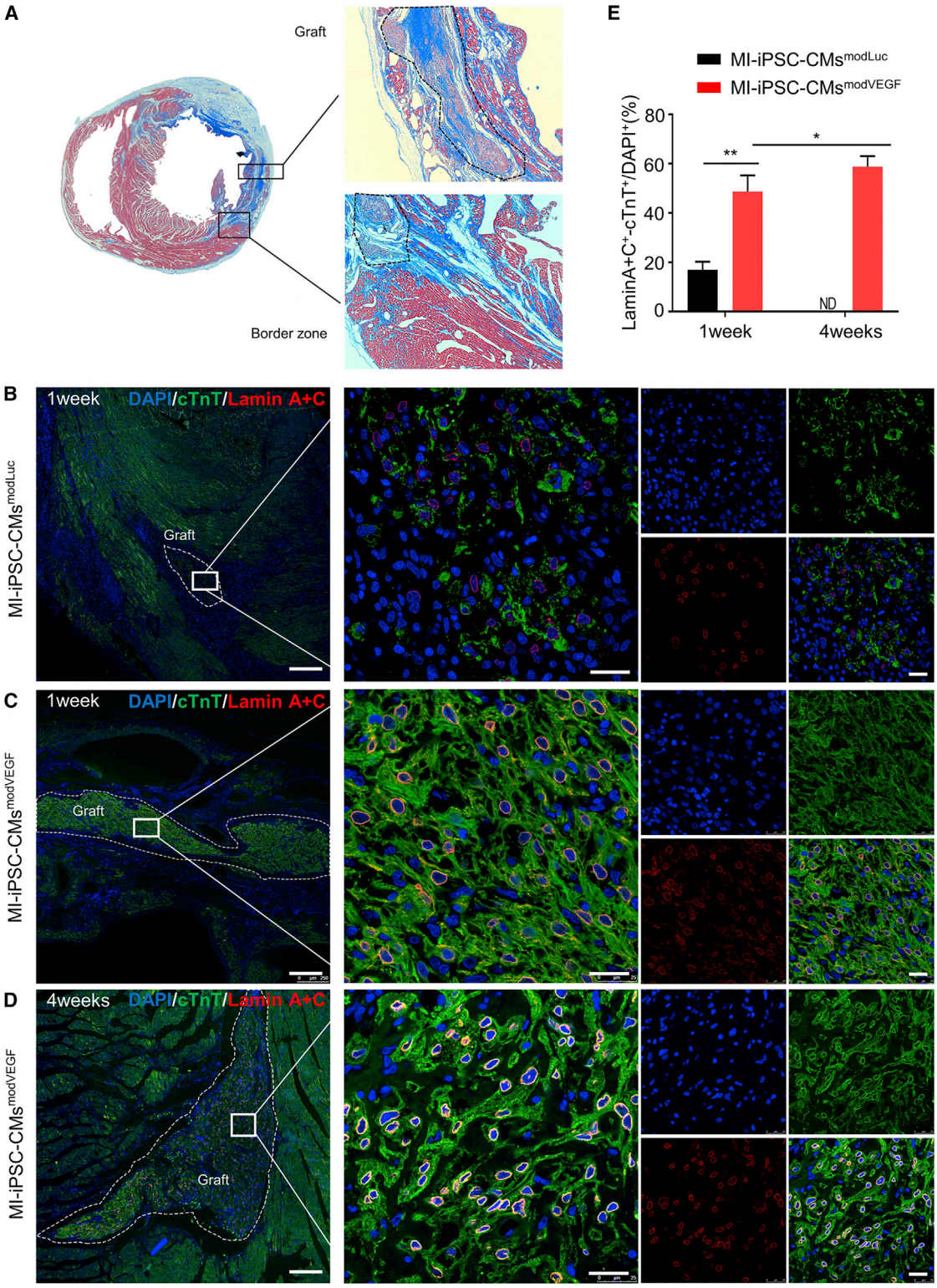

Figure 2. modVEGF-transfected iPSC-CMs exhibit significantly improved engraftment

(A) Masson's trichrome staining of rat hearts subjected to myocardial infarction (MI) and transplantation of iPSC-CMs^{modVEGF}. Remuscularization of the infarct region with iPSC-CMs at 4 weeks post engraftment. (B–D) Representative confocal immunofluorescence images of rat hearts subjected to MI and transplantation of iPSC-CMs 1 week

(legend continued on next page)

To further ensure that the VEGF protein secreted by the modVEGF-treated iPSC-CMs was functional, we tested whether the conditioned medium could promote key angiogenic properties on human umbilical vein endothelial cells (HUVECs) *in vitro*. Based on a tube formation assay, we found a favorable response when employing the conditioned medium from the iPSC-CMs^{modVEGF} group to induce significantly increased tubular-like structures compared with the control group (Figures S5A and S5B). In addition, we also noted a significantly more favorable response from the conditioned medium taken from the iPSC-CMs^{modVEGF} group to promote proliferation and migration of HUVECs in a scratch-wound healing experiment (Figures S5C and S5D). Taken together, these results indicated that modVEGF-transfected iPSC-CMs elicited strong angiogenic properties *in vitro*, which further supported their therapeutic potential for cardiac cell therapy.

RNA sequencing reveals activated gene networks following modVEGF transfection

Using RNA sequencing and analysis we compared the global gene expression profiles of modVEGF-treated iPSC-CMs and control iPSC-CMs (iPSC-CMs transfected with luciferase mRNA [modLuc], denoted iPSC-CMs^{modLuc}). Differentially expressed genes (DEGs) between the iPSC-CMs^{modVEGF} group and the iPSC-CMs^{modLuc} group were revealed by 3 days post modRNA transfection (Figures 1H; and S6A). Upregulated and downregulated genes were subjected to Gene Ontology (GO) enrichment analysis and Kyoto Encyclopedia of Genes and Genomes (KEGG) pathway enrichment analysis. According to GO and KEGG analysis, cell growth, metabolism, and extracellular matrix-related genes were enriched in the iPSC-CM^{modVEGF} treatment group, along with the phosphoinositide 3-kinase (PI3K)-protein kinase B (Akt) and advanced glycation end products (AGE)-receptor for AGE (RAGE) signaling pathways (Figures S6B and S6C). These significantly enriched signaling pathways included the upregulation of genes such as VEGFA, PIK3R5, SOX2, FLT1, ACTN1, MYLK, and MMP2 (Figures 1H and 1I). The GO and KEGG analysis revealed enrichment of cardiac muscle contraction-related genes and adrenergic signaling pathways in the downregulated genes (Figures S6D and S6E). The *in vitro* RNA sequencing results indicated dynamic changes in gene expression profiles of the modVEGF-treated iPSC-CMs. These changes may better promote CM proliferation, intercellular adhesion, intracellular signaling, and negatively regulate inflammation, which may collectively increase engraftment capacity.

iPSC-CMs pre-treated with modVEGF mRNA significantly improve the survival rates of transplanted cells

We next investigated the ability for modVEGF-transfected iPSC-CMs to engraft in host myocardium in a rat model of MI (Figure S7A). All the rats undergoing surgery presented with transmural MIs, and our model consistently provided infarct sizes around 35% of the left ventricle (Figures S7B–S7D and SV2). All rats receiving iPSC-CM^{modVEGF} treatment revealed extensive remuscularization in the infarcted areas (Figure 2A). To visualize and compare engraftment between iPSC-CMs^{modVEGF} with control iPSC-CMs^{modLuc}, we next performed Lamin A + C staining on tissue sections taken along the grafted region within and adjacent to the border zone (Figures 2B–2D and S8). In both the iPSC-CMs^{modLuc} and iPSC-CMs^{modVEGF} treatment groups, surviving transplanted cells could be found 1 week post transplantation. Of interest, a significantly larger percentage of modVEGF-treated iPSC-CMs had engrafted in the infarcted tissue compared with the iPSC-CMs pre-treated with modLuc. Additionally, the majority of the human cells were located in the infarct region and border zone myocardium, which suggested minimal migration following injection (Figures 2B, 2C, S8A, and S8B). At 4 weeks post infarction and transplantation, no trace of iPSC-CM^{modLuc} cells were found in the injured rat hearts. On the contrary, a large percentage of iPSC-CM^{modVEGF} cells were still detectable in the infarct region and border zone at 4 weeks post infarction and transplantation (Figures 2D and S8C), and the density of the transplanted iPSC-CMs increased significantly compared with engraftment rates seen at 1 week post transplantation (Figure 2E).

In order to eliminate excessive inflammation and immune surveillance as possible causes for the discrepancy of cell survival seen between the groups, we investigated the tissue-specific immune responses in each group, taking an immunohistology approach against macrophage marker CD68 and T lymphocyte marker CD3. We found that the oral administration of immunosuppressive agents was efficient to alleviate transplant rejection of the grafted cells, as made evident by the compromised infiltration of immune cells in iPSC-CMs-treated groups (Figures S9A–S9D).

Cardiac transplantation of modVEGF mRNA-treated iPSC-CMs promotes enhanced functional properties in the infarcted rat heart

To confirm whether the VEGF modRNA-engineered iPSC-CMs influenced left ventricular (LV) function, we performed serial echocardiography measurements following injury and cell transplantation. Specifically, we established five experimental groups, namely the Sham group, the MI group, the MI group treated with Matrigel (MI-Matrigel group), the group employing iPSC-CMs loaded with modLuc, and the iPSC-CMs loaded with modVEGF. In line with the schematic diagram of the experimental design (Figure S7A), echocardiography was performed prior to MI and cell delivery, and then at

(B and C) or 4 weeks (D) after engraftment: green, cTnT; red, Lamin A + C; blue, DAPI. Note the increased graft size seen in iPSC-CMs^{modVEGF}-treated groups at 1 week (C) and 4 weeks (D) post transplantation. CMs treated with modVEGF display greater structural integrity post transplantation as made evident by Lamin A + C staining (C and D). Scale bars: 250 μm. Scale bars (zoomed snapshot), 25 μm. (E) Quantitative analysis of the survival of iPSC-CMs in the host heart at 1 week and 4 weeks post MI and iPSC-CMs transplantation. The survival of iPSC-CMs can be detected in both groups at 1 week post transplantation, but only CMs from the MI-iPSC-CMs^{modVEGF} group at detected at 4 weeks post transplantation. 1 week, MI-iPSC-CMs^{modLuc} n = 3, MI-iPSC-CMs^{modVEGF} n = 3; 4 weeks, MI-iPSC-CMs^{modLuc} n = 7, MI-iPSC-CMs^{modVEGF} n = 5. All data are means ± SD; ND, not detected; *$p < 0.05$, **$p < 0.01$.

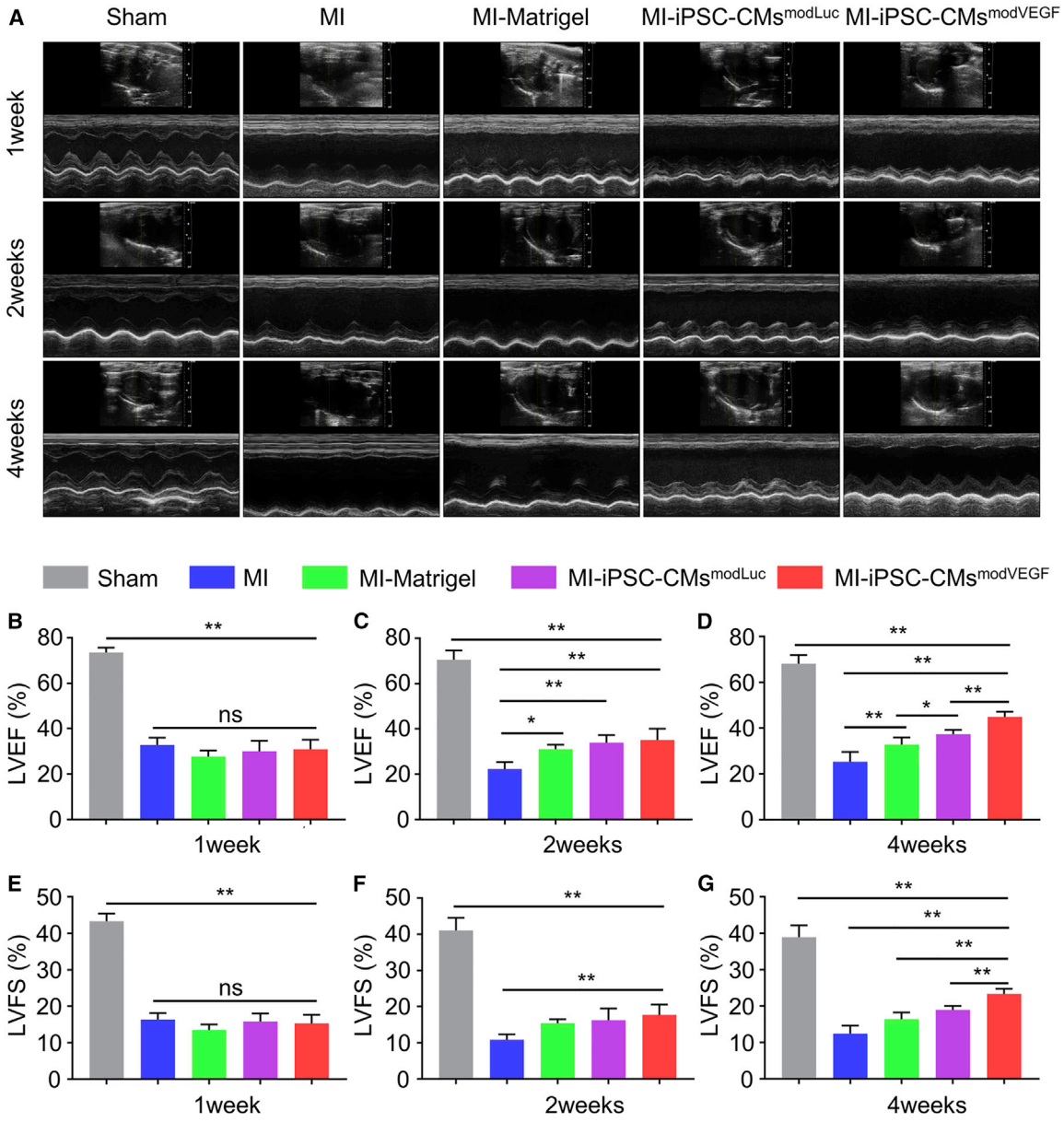

Figure 3. Recovery of rat heart function following iPSC-CMs transplantation

(A) M-mode echocardiogram tracings representing each group at 1, 2, and 4 weeks after infarction and cell transplantation. (B–D) LVEF at 1 week (B), 2 weeks (C) and 4 weeks (D) following MI and treatment. (E–G) LVEF at 1 week (E), 2 weeks (F) and 4 weeks (G) following MI and treatment. LVEF, left ventricular ejection fraction; LVFS, left ventricular fractional shortening. Sham, n = 4; MI, n = 3; MI-Matrigel, n = 3; MI-iPSC-CMs^{modLuc}, n = 5; MI-iPSC-CMs^{modVEGF}, n = 5. All data are means ± SD. NS indicates $p > 0.05$, $^{*}p < 0.05$, $^{**}p < 0.01$.

7 days, 14 days, and 28 days post MI and cell replacement therapy (Figure 3A).

Echocardiography revealed similar levels of decreased LV function between all the groups receiving MI at 1 week post MI injury (Figure 3B). Statistical analysis performed using cardiac ultrasound detection showed that there was no significant difference in LV ejection fraction (LVEF) and LV fractional shortenings (LVFS) between the experimental group and each control group in the first week of infarction and treatment (Figures 3B and 3E). However, 2 weeks post MI and treatment, the LVEF and LVFS in the rats receiving iPSC-CMs^{modVEGF} were significantly increased over other experimental groups (Figures 3C and 3F). By the fourth week, LV heart function was dramatically improved in the rats receiving iPSC-CMs^{modVEGF},

where LVEF improved from 30.9% ± 4.2% to 44.9% ± 2.3% and LVFS improved from 15.3% ± 2.4% to 23.4% ± 1.4%. LV function in rats treated with iPSC-CMs^{modVEGF} was significantly higher than that of the rats receiving iPSC-CMs^{modLuc} treatment, which saw only subtle improvements in LVEF from 30.1% ± 4.5% at 1week post MI to 37.4% ± 1.9% at 4 weeks post MI, as well as subtle increases in LVFS from 15.8% ± 2.2% at 1week post MI to 19.0% ± 1.1% at 4 weeks post MI (Figures 3D and 3G). Both cell treatment groups outperformed non-cell-based treatments and controls. The echocardiogram parameters were significantly improved in rats treated with iPSC-CMs^{modVEGF} and thus support the therapeutic potential of mRNA-enhanced iPSC-CMs as a novel cardiovascular cell therapy to improve cardiac function.

iPSC-CMs^{modVEGF} treatment reduces myocardial fibrosis and preserves ventricular wall thickness

To further assess the tissue morphology of the infarcted rat hearts following cell transplantation, hearts were harvested 4 weeks post MI and treatment. Initial inspection of the gross morphology of the rat hearts treated with iPSC-CM^{modVEGF} revealed smaller areas of blanching and injury compared with the other treatment groups (Figures S10A and S10B). Hematoxylin-eosin staining and analysis confirmed a significantly larger portion of extensive tissue regeneration in the group undergoing MI and transplantation with iPSC-CMs^{modVEGF} (MI-iPSC-CMs^{modVEGF}) compared with other treatment groups (Figure 4A). The MI-iPSC-CMs^{modVEGF} treatment group presented with larger surviving grafts in the border zone of the infarction, and the CMs appeared elongated and matured (Figures S11A–S11E). LV scar sizes, detected by Masson's trichrome staining and quantitative analysis, were significantly smaller in the MI-iPSC-CMs^{modVEGF} group, which also presented with well-maintained wall thickness (Figures 4B–4E). Vimentin staining indicated a large presence of fibroblasts in the infarcted region in most groups at 4 weeks post MI and injury. However, the number of infiltrating fibroblasts found in the MI-iPSC-CMs^{modVEGF} treatment group was significantly less compared with other treatment groups (Figures 4F and 4G). Taken together, iPSC-CMs^{modVEGF} treatment following MI injury partially reduced the fibrotic area and prevented extensive myocardial thinning and cardiac dilation.

Transplantation of iPSC-CMs pre-treated with modVEGF mRNA exhibits *in situ* proliferation and maturation

We next sought to explore cell vitality post transplantation. As shown in Figures 1H and 1I, a major difference in the gene expression profiles between the untreated iPSC-CMs and the modVEGF mRNA-transfected iPSC-CMs was the increased expression patterns of genes involved in cell-cycle regulation. We therefore assessed to what level the administered iPSC-CMs remained proliferative up to 4 weeks post transplantation. As shown by Ki67 staining and analysis, we found that the proliferation rate of CMs from the MI-iPSC-CMs^{modVEGF} group was significantly higher than CMs found in the MI-iPSC-CMs^{modLuc} group at 1 week post transplantation (Figures 5A, B, and D). However, the expression of Ki67 within the transplanted iPSC-CMs decreased significantly at 4 weeks post transplantation (Figures 5B–5D). Of interest, very few Ki67-positive CMs could be localized in the host myocardium adjacent to grafted iPSC-CMs, indicating that the proliferative effects of VEGF mRNA mainly work on the transplanted CMs rather than extending to the adult resident CMs (Figures 5E–5H). These data suggested that iPSC-CMs conditioned with modVEGF elicit a strong, acute proliferative response to the administered cells following *in vivo* delivery and engraftment, which may prolong graft survival.

Subsequently, we investigated to what extent modVEGF treatment could enhance maturation properties of the administered iPSC-CMs *in situ*. The immunophenotype of grafted myocardium from the iPSC-CMs^{modVEGF} group revealed stronger MLC2v expression and greater sarcomeric structure and alignment compared with the iPSC-CMs^{modLuc} group (Figures S12A–S12F). Interestingly, grafted CMs from both the iPSC-CMs^{modVEGF} and iPSC-CMs^{modLuc} transplantation groups expressed the cardiac gap junction protein connexin 43 (Cx43). Grafted myocardium from the iPSC-CM^{modLuc} group expressed relatively low levels of Cx43 between neighboring CMs, which was limited to occasional areas within the graft (Figure 6A). By contrast, iPSC-CMs^{modVEGF} grafts strongly expressed Cx43, which increased significantly over time and could be detected throughout most regions of the grafted myocardium (Figures 6B and 6C). However, Cx43^{+} gap junctions were not visualized between the transplanted human iPSC-CMs and the host rat myocardium at the graft-host contact points (Figures S13A–S13E). Nevertheless, the combination of a declining fraction of Ki-67^{+} CMs with increased Cx43 expression at 4 weeks post administration within the graft may indicate continued maturation of the transplanted iPSC-CMs^{modVEGF}.

Transplantation of modVEGF-treated iPSC-CMs enhances angiogenesis *in vivo*

Previous studies reported the recruitment of host blood vessels within zones of engraftment following the transplantation of neonatal CMs or cardiac progenitors,[37,38] respectively. An enhanced vascular network within the newly generated myocardial graft is essential for long-term survival. Thus, to assess the angiogenic capacity of VEGF modRNA-treated iPSC-CMs to stimulate neovascularization within the grafted region, we performed CD31 and α-SMA staining and analysis.

Grafts from the iPSC-CMs^{modVEGF} treatment group gave rise to an extensive network of capillaries and mature, stable arterioles within 1 week of administration (Figure S14A). These networks of capillaries and arterioles remained at least until our experimental endpoint, reflecting continual angiogenesis at 4 weeks post MI and transplantation (Figure S14B). The vasculature identified within the grafted region *in vivo* was derived from the host, as made evident by immunohistochemistry staining with species-specific antibodies (Figure S14C). Far fewer blood vessels could be visualized in the grafts from the iPSC-CMs^{modLuc} treatment group, as the majority of grafts were not detected by the fourth week. The MI-iPSC-CM^{modVEGF} group revealed a significant increase in capillary densities within the infarcted regions of the heart compared with other treatment groups (Figures 7A, 7C, and 7D). Of interest, a

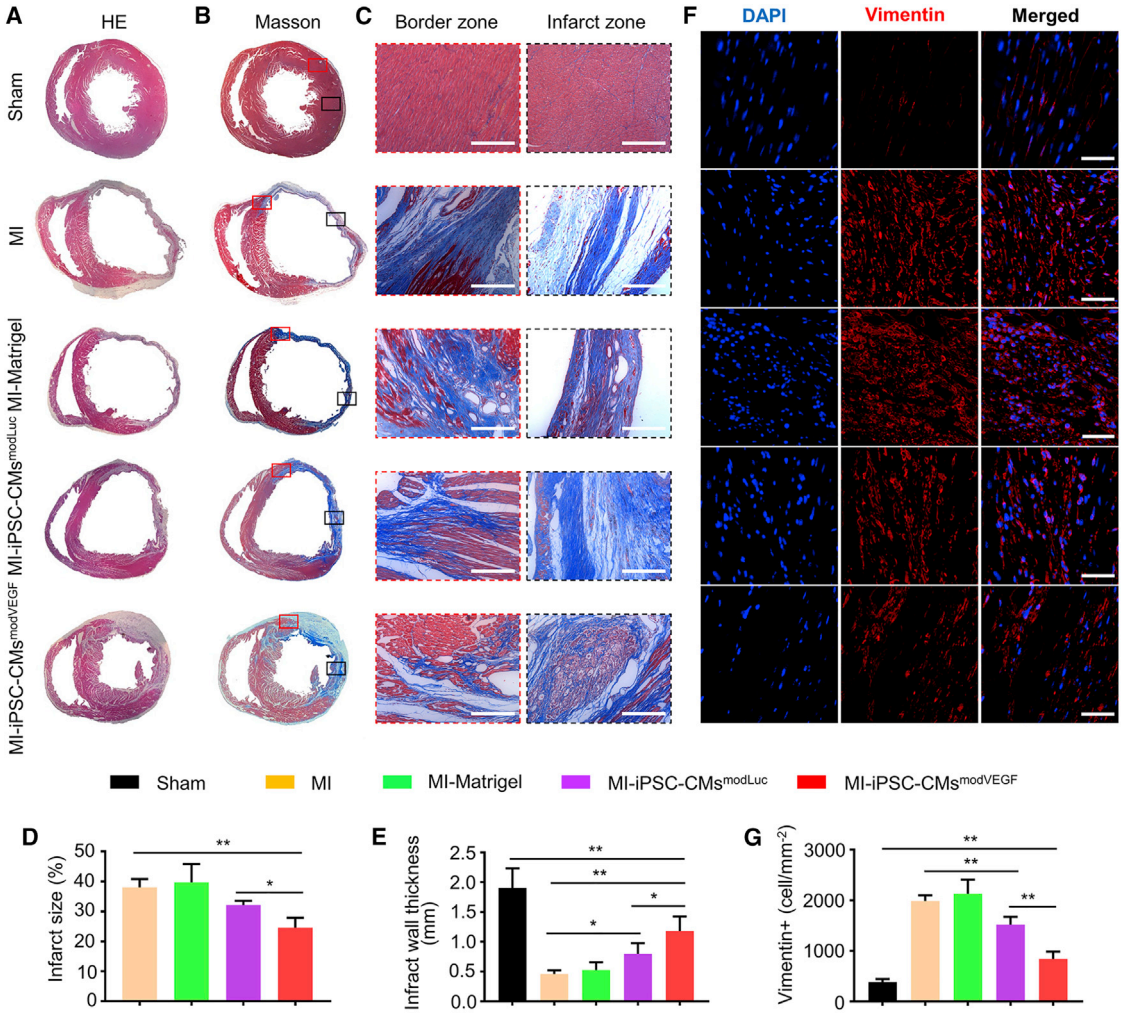

Figure 4. Morphological analysis of the ventricular myocardium following MI and iPSC-CMs treatment

Representative photographs of transverse sections taken through the ventricular myocardium of infarcted rat hearts at 4 weeks post MI and iPSC-CMs transplantation, stained with hematoxylin-eosin (A) and Masson's trichrome (B). Note: images depict infarction zone of the LV wall in different treatment groups. The red squares (B) indicate the border zones and the black squares indicate the infarction zones. Note: the image in the bottom row in Figure 4B is reproduced from Figure 2A to illustrate the reduced fibrotic area in relation to the newly grafted myocardium. (C) Representative Masson's trichrome-stained partial enlarged view of border zone and infarct zone in each group. There is obvious collagen fiber (stained in blue) between the surviving CMs in the border zone. Scale bar, 100 μm. (D) Quantitative analysis and comparison of the infarct zone of each group; note reduced infarct sizes in MI-iPSC-CMs^{modVEGF} group. (E) Quantitative analysis and comparison of LV wall thickness in each group, note LV wall thickness in the MI-iPSC-CMs^{modVEGF} group was significantly larger. (F) Representative photomicrographs of the infarcted rat ventricles from each group, immunolabeled with vimentin. Scale bar, 50 μm. (G) Quantitative analysis of the density of vimentin-positive cells in each group; the density of vimentin-positive cells in the MI-iPSC-CMs^{modVEGF} group was significantly lower. n = 5. All data are means ± SD; *p < 0.05, **p < 0.01.

greater number of newly formed vessels within the infarct zone of rat hearts treated with iPSC-CM^{modVEGF} were double positive for both CD31 and α-SMA, an indication of vascular tube stabilization and non-leaky vessel formation (Figures 7A, 7C, and 7D). We also performed CD31 and α-SMA staining and analysis along the infarct border zone and found that the rat hearts receiving iPSC-CM^{modVEGF} treatment demonstrated significant increases in capillary and arteriole densities, compared with all other treatments (Figures 7B, 7E, and 7F).

DISCUSSION

In this study, we evaluated the potential for modVEGF-treated iPSC-CMs to enhance cell survival following cardiac transplantation. We hypothesized that VEGF mRNA-engineered iPSC-CMs could better prevent adverse ventricular remodeling events following acute MI than conventional iPSC-CMs. A large number of studies have previously shown that pluripotent stem cell (PSC)-derived CM replacement therapy has a beneficial therapeutic effect in animal models of heart disease and HF.[13,39-43] Herein, we transplanted and assessed

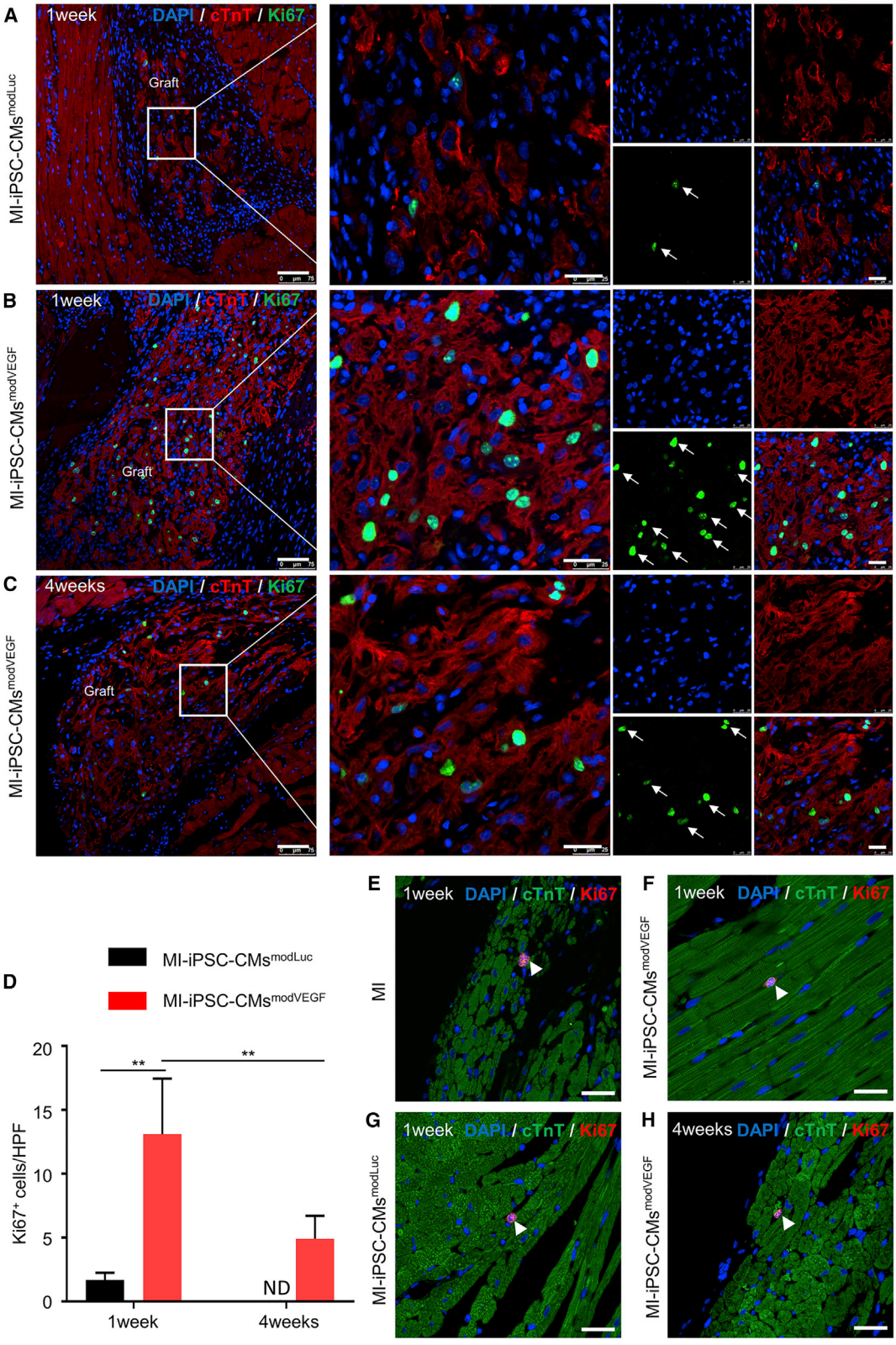

(legend on next page)

the function of relatively immature iPSC-CMs, based on CM structure and marker gene expression profiles. Some dispute exists in the literature whether more mature and structurally advanced iPSC-CMs could generate more efficient grafting capabilities when transplanted *in vivo*.[11] Importantly, the underdeveloped electrophysiological properties of the immature CMs are recognized as a major caveat limiting electromechanical integration, likely leading to arrhythmias post engraftment.[44] The application of maturated iPSC-CMs may solve electrophysiological issues; however, studies have shown mature CMs are brittle and prone to cell death under manipulation and transplantation.[43,45] For example, Reinecke H et al. showed that mature adult CMs were unable to survive when transplanted to the damaged myocardium, while immature fetal and neonatal CMs presented with greater survival rates.[45] In our studies, we found that *in vitro* cell manipulation was well tolerated among the immature iPSC-CMs (Figure 1 and S4). Moreover, the VEGF modRNA transfected CMs gave rise to larger grafts than unmodified CMs at 4 weeks post administration (Figure 2), indicating significant survival and growth *in vivo*, likely homage to their enhanced proliferative features (Figure 5).

We speculate that the global cardiac functional improvement stemming from the cell transplantation in our study was mainly stimulated by paracrine effects and added mechanical support rather than synchronous beating between the transplanted cells and recipient cardiac muscle (Figure 3).[46,47] Engrafted iPSC-CMs appeared to be non-integrated with the host myocardium (Figures 6 and S13), a phenomenon that may be attributable to the physiological differences between the different species as well as the physical impedance of the scar tissue.[14] Although we did not explore to what extent iPSC-CMs^{modVEGF} transplantation had on non-fatal ventricular arrhythmias, this assessment has been explored more intensively in non-human primate and large animal models of cardiac injury.[15,48,49]

Boosting the properties of immature iPSC-CMs with transiently overexpressed mRNAs to enhance their engraftment, function, and maturity is a tantalizing concept that could lead to a quicker and more cost-efficient clinical approach. As demonstrated herein, grafts formed from the iPSC-CMs treated with modVEGF showed significant maturation *in vivo*. Interestingly, only about 20% of our differentiated CMs expressed MLC2v prior to transplantation (Figure S3), yet the vast majority of iPSC-CMs^{modVEGF} at 4 weeks post engraftment upregulated Cx43 expression and expressed MLC2v (Figures 6B–6D and S12D–S12F). More evidence is needed to determine optimal maturity of iPSC-CMs for cell transplantation and regenerative therapy, and future studies should address how CM maturation augments engraftment and survival rates of the transplanted cells.[50-53]

In order to better promote the survival of transplanted cells in the heart, alternative approaches have employed survival cocktails along with "super-dose" cell injections.[13,49] Such methods increase cost of goods/treatment, and the complex formulation may add risk to the therapeutic procedure. Nonetheless, a vast majority of studies employing cardiac cell therapies showcase the gradual disappearance of cells, which likely become apoptotic resulting in an unsatisfactory myocardial tissue graft.[49,54,55] For example, in a study by Zhu et al., human pluripotent stem cell-derived cardiovascular progenitor cells (hPSC-CVPCCs) were delivered to non-human primate hearts and a small number of transplanted cells were found to survive 1 week after transplantation; however, at 28 days post administration, very few cells were detected.[49] Of interest, all of the rats receiving iPSC-CMs^{modVEGF} treatment in our study retained myocardial cell grafts up to 4 weeks post MI and transplantation, our study endpoint (Figures 2, S11, and S12). On the contrary, graft survival was negligible in all rats receiving iPSC-CMs^{modLuc} treatment at 4 weeks post surgery and cell transplantation. Indeed, far fewer CMs from the iPSC-CM^{modLuc} group were found to survive only 1 week post injury and transplantation, compared with those of the VEGF-treated iPSC-CMs. This may seem at odds with other studies that report the survivability of iPSC-CMs in rodent models for at least 8 weeks following cardiac transplantation.[14,42,56,57] However, the vast majority of these studies directly injected 10×10^6 CMs or more to the rat hearts, whereas we chose to employ only 5×10^6 CMs and follow the transplants acutely. Furthermore, it could be argued that a more effective immunosuppression regimen is needed in these studies. Indeed, the administrative doses, appropriate recipe of agents, and timings of administration are essential to improving iPSC-CM engraftment in rodent models of cardiovascular ischemic injury. Nevertheless, the robustness of the VEGF-treated iPSC-CMs to engraft, overcome transplantation failure, and improve cardiac function adds further credence to this regimen.

Several different delivery strategies accompany the administration of iPSC-CMs for cardiac regeneration, including injecting the cells as single cells or transplantation with biomaterials.[15,58,59] In our study, we employed Matrigel, an injectable matrix biopolymer, as a carrier to enhance structural support of the injected cells. Direct injections of Matrigel to the rodent heart have previously been shown to

Figure 5. modVEGF-treated iPSC-CMs retain proliferation capacity following transplantation in infarcted rat hearts

(A and B) Comparison of Ki67 immunostainings of engrafted CMs from MI-iPSC-CMs^{modLuc} (A) or MI-iPSC-CMs^{modVEGF} (B) 1 week post transplantation: red, cTnT; green, Ki67; blue, DAPI. (C) Representative confocal immunostaining of cTnT and Ki67 double-positive cells in the MI-iPSC-CMs^{modVEGF} group at 4 weeks post transplantation. The white arrows indicate nuclear presence of Ki67. (A–C), Scale bars: 75 μm. Scale bars (zoomed snapshot), 25 μm. (D) Quantitative analysis and comparison of Ki67 positive cells at 1 and 4 weeks between the MI-iPSC-CMs^{modLuc} group and MI-iPSC-CMs^{modVEGF} group. (E–H) Comparison of Ki67 immunostainings of host myocardial tissue following administration of MI (E) or MI-iPSC-CMs^{modLuc} (F) or MI-iPSC-CMs^{modVEGF} (G) 1 week post transplantation: green, cTnT; red, Ki67; blue, DAPI. (H) Representative confocal immunostaining of cTnT and Ki67 double-positive cells in the MI-iPSC-CMs^{modVEGF} group at 4 weeks post transplantation. The white arrows indicate nuclear presence of cTnT and Ki67 double-positive cells. (E–H) Scale bars, 25μm. 1 week, MI-iPSC-CMs^{modLuc} n = 3, MI-iPSC-CMs^{modVEGF} n = 3; 4 weeks, MI-iPSC-CMs^{modLuc} n = 7, MI-iPSC-CMs^{modVEGF} n = 5. All data are means ± SD. ND, not detected; *$p < 0.05$, **$p < 0.01$.

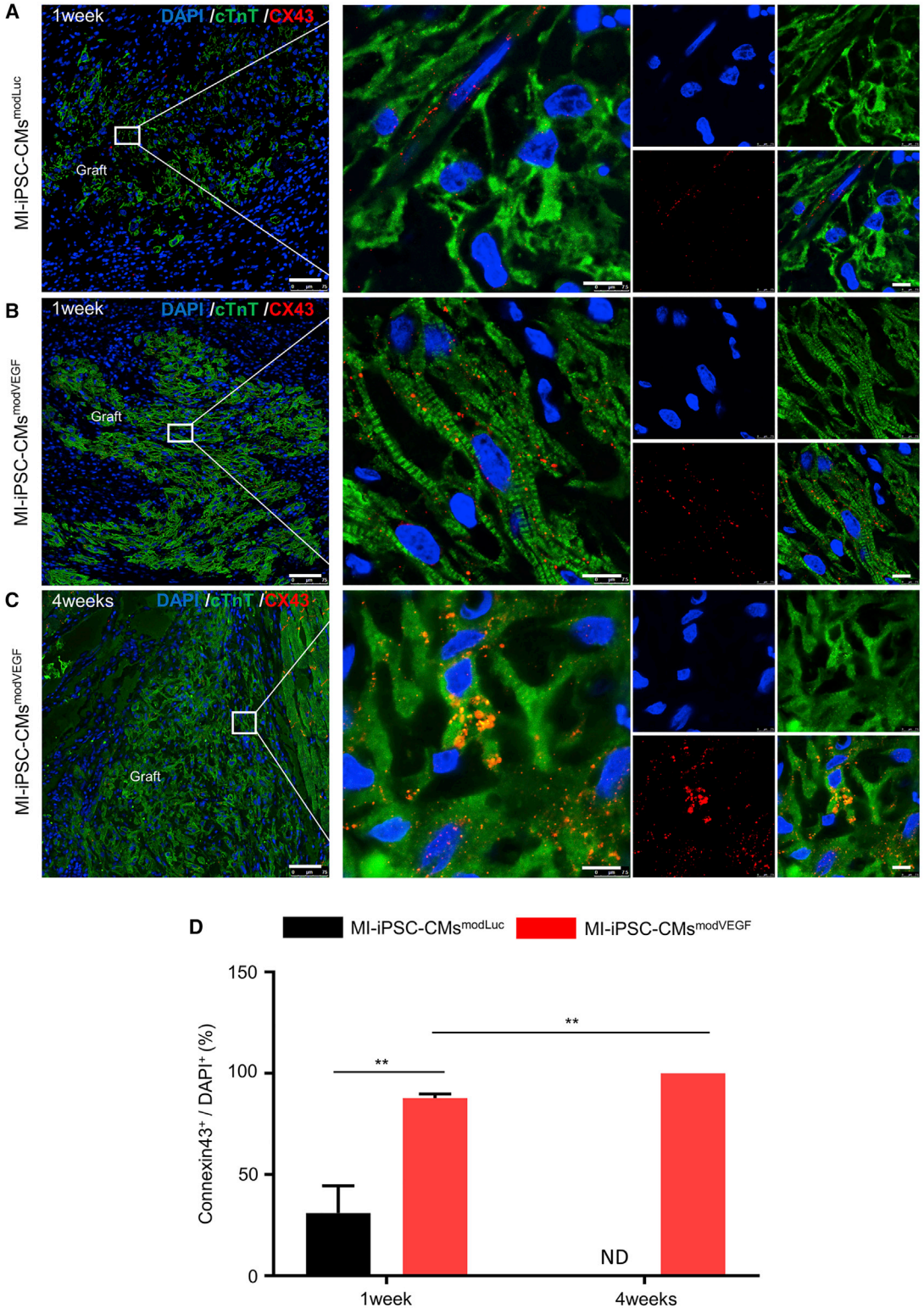

Figure 6. modVEGF-transfected iPSC-CMs exhibit maturation with time from engraftment

(A–C) Representative confocal immunofluorescence staining of connexin 43 (Cx43) in the grafted region of infarcted rat myocardium following iPSC-CMs^{modLuc} transplantation at 1 week (A) or iPSC-CMs^{modVEGF} transplantation at 1 week (B) and 4 weeks (C): green, cTnT; red, Cx43; blue, DAPI. Note MI-iPSC-CMs^{modVEGF} treatment

(legend continued on next page)

improve cardiac function, which was also noted in our study (Figures 3B–3G).[60] Some of the previously mentioned reports and others often show variation in LV function following treatment. In our study a consistent and stable increase in LV cardiac function was recorded with limited variability following the delivery of iPSC-CMs^{modVEGF} (Figure 3).

The intramyocardial administration of VEGF mRNA has recently been shown to limit myocardial damage in a large animal model of cardiac injury.[29] As VEGF acting on VEGF receptor (VEGFR)-1 and VEGFR-2 mediates inflammation, it has been suggested that VEGF signaling compensates for the effects of hypoxia to protect the injured myocardium.[61]

The expression kinetics of VEGF mRNA coincides with the pathophysiological onset of MI, during which the hypoxic/ischemic injury induces a surge of cell death and apoptosis acutely, followed by an intense inflammatory reaction sub-acutely. It is very likely that the rapid, pulse-like secretion of VEGF protein from the mRNA-enhanced iPSC-CMs not only led to the rapid vascularization of the infarcted myocardium but also provided inflammatory protection to the damaged ventricle. Taken together, the VEGF-secreting CMs prevented progressive remodeling and achieved long-term functional benefits (Figure 4).

Of further interest was the bulk RNA sequencing and analysis of iPSC-CMs treated with modVEGF mRNA that led our attention to the upregulation of several genes related to cell proliferation (Figures 1H and 1I; Figure S6). Further KEGG pathway analyses revealed significant upregulation of the PI3K-Akt and AGE-RAGE signaling pathways in the iPSC-CMs^{modVEGF} group. AGE-RAGE promotes mechanisms of cell growth, angiogenesis, and proliferation through nuclear factor κB (NF-κB) activation.[62] Several studies have shown the activation of the PI3K-Akt signaling pathway relates to cell proliferation and migration.[63-65] We therefore investigated whether the iPSC-CMs^{modVEGF} maintained pro-proliferative kinetics *in situ* following intramyocardial injection. Using an antibody directed against Ki67, we detected a large percentage of CMs from the iPSC-CMs^{modVEGF} group undergoing mitosis, following transplantation and engraftment within the host myocardium (Figure 5). The ability for VEGF to directly promote cardiac muscle hyperplasia has been reported in alternative model systems of heart repair.[66] We cannot categorically claim modVEGF transfection alone directly promoted expansion of our transplanted human iPSC-CMs in rat myocardium. However, the treatment of iPSC-CMs with VEGF mRNA led to the significant increase in the number of structurally matured CD31$^+$/α-SMA$^+$ vessels (Figures 7 and S14). One could speculate that the extensive neovascularized networks we visualized within the grafted regions and border zones stemming from iPSC-CM^{modVEGF} treatment could be fueling the CM patches with alternative myogenic stimuli.

From a cell therapy perspective, the regeneration of critically damaged myocardial tissue requires vascularized muscle. Alternative approaches to vascularize cardiac tissue have included the overexpression of VEGF in alternative cell types,[67] or co-differentiation strategies that result in the application of a mixed population of CMs and endothelial cells.[68] In our study, the use of VEGF-secreting iPSC-CMs alleviated the need to deliver multiple cell types for advancing a vascularized muscle patch. The approach to transiently overexpress VEGF protein from mRNA-enhanced iPSC-CMs was not compared with alternative, permanently integrated technologies. For example, although the manipulation of iPSC-CMs with DNA-based methods may result in more blood vessel formation, the extended exposure of VEGF could lead to vessel permeability, cardiac edema, and even vascular tumors increasing the undesirable mortality of the host recipients, as demonstrated by earlier reports.[28,69,70] Hence, modRNA provides an effective approach to control the spatial and temporal gene expression and determines its biological outcomes in cardiac repair after injury.

In summary, we demonstrated for the first time a combinatorial treatment regimen employing novel modRNA technologies with cardiac cell therapies. VEGF modRNA loading of iPSC-CMs significantly improved the survival of transplanted CMs, which also promoted the recovery of cardiac function after acute MI. As shown in Figure 8, we are optimistic about the future applications that unite modRNA technologies with cardiac cell therapies for the treatment of HF. Modified mRNA technologies can further promote the application of cell therapy in this field.

MATERIALS AND METHODS

Generation and maintenance of CMs

Human iPSC cell line reprogramming from human cord blood cells was a kind gift from Professor Yanxin Lee's group (Shanghai Children's Medical Centre, School of Medicine, Shanghai Jiaotong University). iPSCs were maintained on Matrigel-coated six-well plate in E8 medium, which was refreshed every day. When cells were 70%–80% confluent, they were dissociated using 5×10^{-4} M EDTA (Gibco) and incubated on another Matrigel-coated six-well plate in E8 medium supplemented with 5 μM Rock inhibitor Y27632 (STEMCELL) for the first 24 h to reduce cell apoptosis. The condition of cell culture was set at 37°C in 5% CO_2.

The induction and generation of CMs from iPSCs was based on the monolayer differentiation method using two well-defined chemicals to regulate Wnt/β-catenin signaling as previously described.[35] In summary, on day −2, iPSCs were dissociated with Accutase

exhibited enhanced Cx43 expression at 1 week and 4 weeks post transplantation, suggesting more gap junctions between cell-cell interfaces. For (A–C), scale bars, 75 μm. Scale bars (zoomed snapshot), 7.5 μm. (D) Quantitative analysis and comparison of Cx43-positive cells at 1 week and 4 weeks post transplantation between MI-iPSC-CMs^{modLuc} group and MI-iPSC-CMs^{modVEGF} group. 1 week, MI-iPSC-CMs^{modLuc} n = 3, MI-iPSC-CMs^{modVEGF} n = 3; 4 weeks, MI-iPSC-CMs^{modLuc} n = 7, MI-iPSC-CMs^{modVEGF} n = 5. All data are means ± SD. ND not detected, *p < 0.05, **p < 0.01.

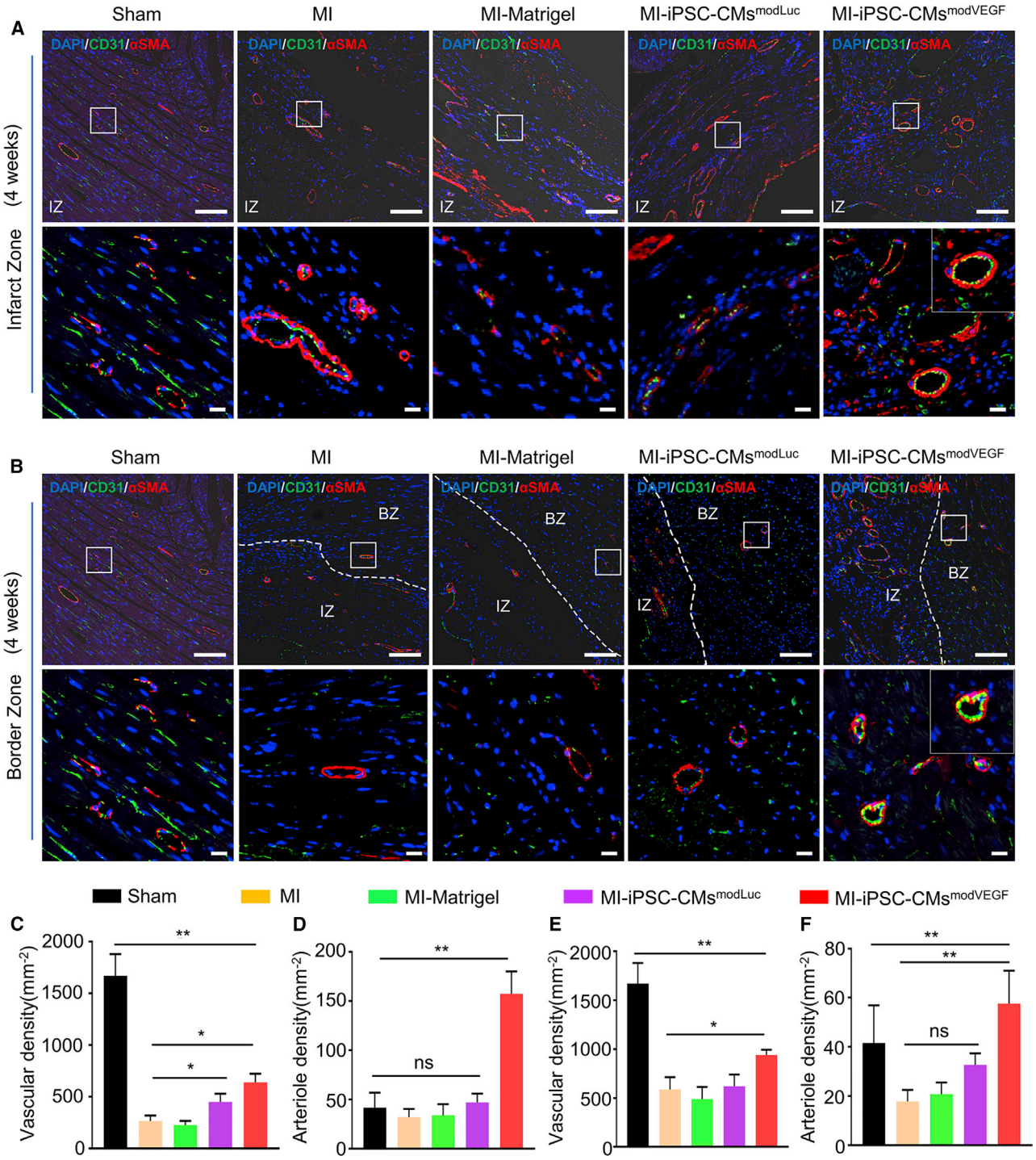

Figure 7. Grafted iPSC-CMs in the rat myocardium within the infarct region and border zone reveal neoangiogenesis 4 weeks post transplantation

(A) Representative confocal images showing the expression of α-SMA and CD31 in the infarct zone (IZ). α-SMA, red; CD31, green; DAPI, blue; n = 5; scale bar, 100 μm; zoom-in scale bar, 15 μm. (B) Representative confocal images showing the expression of α-SMA and CD31 in the border zone (BZ). α-SMA, red; CD31, green; DAPI, blue; scale bar, 100 μm; zoom in scale bar, 15 μm. Note: the images in the left panel in (7A) and (7B) are identical since there is no infarct or border zone in the Sham group. (C and D) Quantitative analysis of CD31-positive capillary density (C) and CD31/α-SMA-positive arteriole density (D) in the infarct zone. (E and F) Quantitative analysis of CD31-positive capillary density (E) and CD31/α-SMA-positive arteriole density (F) in the border zone. All data are means ± SD. NS indicates $p > 0.05$, *$p < 0.05$, **$p < 0.01$.

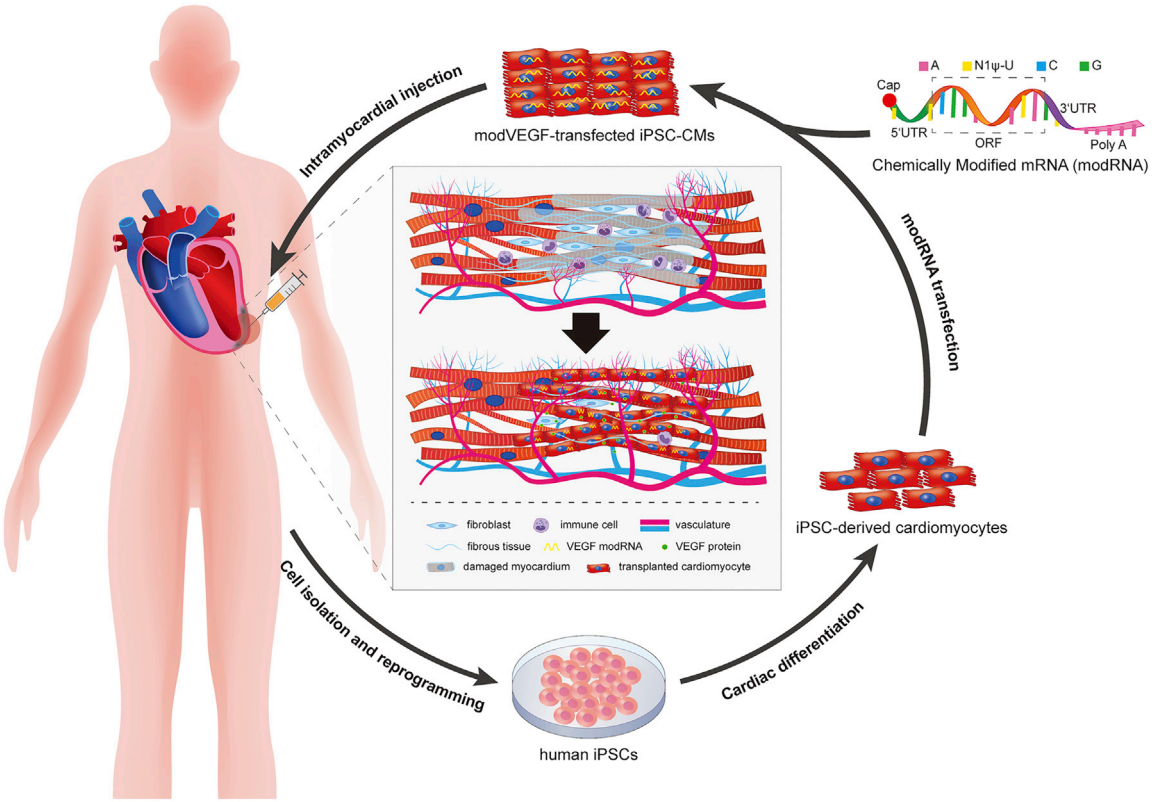

Figure 8. Schematic diagram illustrates the clinical feasibility of modRNA-treated iPSC-CMs for advancing heart repair

(STEMCELL) and seeded onto Matrigel-coated 12-well plates at a density of 1×10^6 cells per well in E8 medium supplemented with 5 μM Y27632. On day −1, culture medium was refreshed. On day 0, once iPSCs reached confluency, CM differentiation was initiated by RPMI 1640 plus B27 minus insulin medium supplemented with 12 μM GSK3β inhibitor CHIR99021 (STEMCELL). The differentiation medium was then replaced with RPMI 1640 plus B27 minus insulin medium after 30 h. On day 3, fresh RPMI/B27 minus insulin medium and conditioned medium at a volume ratio of 1:1 supplemented with 5 μM Wnt inhibitor IWP2 (STEMCELL) was added into each well of Matrigel-coated 12-well plates. On day 5, culture medium was replaced with refresh RPMI/B27 minus insulin medium again. On day 7 and afterward, culture medium was refreshed with RPMI 1640 plus B27 medium every 2 days.

Immunocytochemistry

Cells were dissociated into single cells and seeded on Matrigel-coated 24-well slides or glass-bottom dishes. After cell attachment, samples were fixed with 4% paraformaldehyde (PFA) for 20min, permeabilized with 0.2% Triton X-100 for 20 min and blocked with 10% goat serum for 2 h at room temperature (RT). Incubation with primary antibodies at 4°C overnight and secondary antibodies at RT for 2 h was used to label the target proteins, while staining with DAPI (1:1,000, Yeasen) for 10 min at RT for nuclei detection. The primary antibodies included α-actinin (A7811, Sigma), MLC2v (ab79935, Abcam), MLC2a (311011, SYSY), cTnT (15513-1-AP, Proteintech), Nanog (3369-1, Epitomics), Oct4 (2876-1, Epitomics), Sox2 (2683-1, Epitomics), and Tra-1-60 (MAB4360, Merck_millipore). Species-specific secondary antibodies conjugated with Alexa Fluor 488 or Alexa Fluor 555 (ab150106 or ab150073, Abcam) were diluted according to manufacturer's instructions. Image detection was performed with a confocal laser scanning microscope (Leica TSC SP8). The number of $MLC2v^+$, $MLC2a^+$, and $cTnT^+$ cells and the length and width of CMs were calculated under Image-pro plus 6.0.

Flow cytometry assessment

CMs were dissociated into single cells using CardioEasy Human Cardiomyocyte Digestive Solutions (CELLAPY, CA2012100) according to the manufacturer's instructions. For intracellular staining, a fixation and permeabilization kit from eBioscience was applied according to manufacturer's instructions. Cells were labeled directly with APC-conjugated cTnT antibody (130-106-689, Miltenyi). Flow cytometry analysis was performed with a BD FACSCanto flow cytometer and FlowJo_V10 software.

Transmission electron microscope

iPSC-CMs on day 18 post differentiation were dissociated into single cells and reseeded onto Matrigel-coated six-well plate for

transmission electron microscopy. It was fixed with 4% paraformaldehyde overnight; dehydrated gradually with 10%, 30%, 50%, 70%, 90%, and 100% ethanol; and dried in a fume hood. The samples were finally stained with uranyl acetate for 40 min at RT and imaged using a transmission electron microscope (Hitachi H-7500).

Electrophysiological recordings

The action potential of iPSC-CMs was detected as previously described.[71] Briefly, CMs were dissociated into single cells, reseeded onto glass-bottom dishes (5×10^4/well), and then placed on the stage of an inverted microscope using an Axopatch 700B (Axon Instruments, Union City, CA, USA) patch-clamp magnifier for all cell patch-clamp recordings at RT. Sharp microelectrodes were manufactured from thin-walled borosilicate glass tubes (Sutter Instruments, Novato, CA, USA) using a Flaming/Brown Micropipette Puller P97 (Sutter Instruments, Novato, CA, USA). After thermal polishing and internal solution filling, the final resistance of the micropipette tip was 2–4 MΩ. Internal solution for the perforated patch contained (in mM) 150 KCl, 2.0 $MgCl_2$, 5.0 EGTA, 10 HEPES, and 2.0 Na_2ATP with a pH of 7.2, and external solution contained (in mM) 130 NaCl, 5.0 KCl, 1.0 $MgCl_2$, 2.0 $CaCl_2$, 20 glucose, 10 sucrose, and 10 HEPES with a pH of 7.4.

modRNA synthesis

mRNA was synthesized using T7 RNA polymerase-mediated transcription from a linearized DNA template, which incorporates generic 5′and 3′ UTRs and a poly(A) tail, as previously described.[12,39,40] During the synthesis procedure, uridine was replaced with N1-methylpseudouridine to enhance the *in vitro* stability and protein translation, which makes it called modRNA. Then modRNA was purified using Ambion MEGAclear kit and treated with Antarctic Phosphatase (New England Biolabs) for 30 min at 37°C to remove residual 5′-phosphates. After repurification and quantification, modRNA was resuspended in 10 mM Tris HCl, 1 mM EDTA at 1 μg/μL for use. Open reading frame sequences used for modRNA production were provided previously for EGFP, firefly luciferase, and human VEGF-A_{165}.[28]

modRNA transfection and evaluation

modRNA was transfected into CMs using MessengerMAX Lipofectamine as manufacturer's instructions (Life Technologies). modRNA and MessengerMAX were separately diluted in serum-free medium Opti-MEM (Gibco) and incubated at RT for 5 min, which were then mixed up and incubated at RT for 15 min to form liposome-modRNA complexes. Cells were transfected with the liposome-modRNA complexes for 4 h in Opti-MEM, after which the transfection medium was replaced by fresh culture medium. Every 4 μg of modRNA and 10 μL of MessengerMax were transfected into nearly 2×10^6 iPSC-CMs for each well of a 12-well plate.

modGFP was used as a tool to analyze the transfection efficiency of modRNA. Briefly, modGFP-transfected CMs were dissociated into single cells with CardioEasy Human Cardiomyocyte Digestive Solutions (CELLAPY, CA201210) and detected with a BD FACSCanto Flow Cytometer.

For modVEGF transfection, conditioned medium was collected at different time points (4 h, 12 h, 24 h, 48 h, 72 h, 96 h, and 1 w) and analyzed by ELISA assay (R&D systems) to quantify the total content and the expression kinetics of VEGF protein. All experiments were conducted with three replicates in each group.

Cell viability analysis

To evaluate the effect of modRNA transfection on CM viability, we used a Calcein-AM/PI cytotoxicity and cell viability staining kit (C2015m, Beyotime). Calcein AM and PI stain live and dead cells respectively. CMs were transfected with modVEGF and incubated with Calcein AM (1:1,000) and PI (1:1,000) at 37°C for 30 min, then observed by fluorescence microscope. The number of Calcein AM-positive (surviving) and PI-positive (dead) cells was counted using Image-pro plus 6.0. All experiments were performed independently with five replicates in each group.

Tube formation assay and wound healing assay

For tube formation experiments, 1×10^5 HUVECs were cultured on Matrigel-coated 48-well plates in 200 μL of conditioned medium from modLuc-transfected or modVEGF-transfected iPSC-CMs. Tube formation was visualized and photographed at 24 h post-treatment by LEICA DMI3000B microscope. The numbers of the tube network were counted using Image-pro plus 6.0. All experiments were performed independently with five replicates in each group.

For wound healing assay experiments, 5×10^5 HUVECs were cultured in six-well plate. Confluent monolayer HUVECs were mechanically injured using a sterile 100-μL pipette tip and then incubated with conditioned medium collected from modLuc-transfected or modVEGF-transfected iPSC-CMs for 24 h. Images were captured with LEICA DMI3000B microscope at 0, 12, and 24 h and were analyzed using Image-pro plus 6.0. All experiments were conducted with five replicates in each group.

RNA sequencing

Following the above transfection protocol, iPSC-CMs on day 18 post differentiation were transfected with VEGF modRNA (iPSC-$CMs^{modVEGF}$) and Luciferase modRNA (iPSC-CMs^{modLuc}) respectively. After 3 days of cell culture, total mRNA was collected and extracted using Trizol (Life Technologies) and sent to Novogene (Beijing, China) for RNA sequencing. Briefly, mRNA was purified from total RNA by using poly-T oligo-attached magnetic beads. mRNA fragmentation was then carried out using divalent cations under elevated temperature in first-strand synthesis reaction buffer (5×). First-strand cDNA was synthesized using random hexamer primer and Moloney murine leukemia virus (M-MuLV) reverse transcriptase, after which mRNA was degraded by RNaseH. Second-strand cDNA synthesis was subsequently performed using DNA polymerase I and deoxy-ribonucleoside triphosphate (dNTP). Remaining overhangs were converted into blunt ends via exonuclease and polymerase

activities. After adenylation of 3′ ends of DNA fragments, adaptor with hairpin loop structure were ligated to prepare for hybridization. To select cDNA fragments of preferentially 370–420 bp in length, the library fragments were purified with AMPure XP system (Beckman Coulter, Beverly, USA). Following PCR amplification, the PCR product was purified by AMPure XP beads, and the library was finally obtained. After the library was constructed, samples were quantified using both the Qubit2.0 fluorometer and the Agilent 2100 bioanalyzer. qRT-PCR was then used to detect and quantify the library again to ensure the quality of the library. After the library inspection was qualified, the different libraries were pooled according to the requirements of effective concentration and target data volume, and then sequenced with Illumina NovaSeq 6000.

Animal model of MI and cell transplantation

The animal care and experiments were conducted according to the guidelines of the Animal Care and Experiment Committee of Shanghai Children's Medical Center. Male Sprague-Dawley rats weighing approximately 200–250 g were provided by Shanghai Jiesijie Laboratory Animal Co. The rats were randomly divided into five groups as follows: (1) Sham group, thoracotomy without ligation; (2) MI group, MI without any treatment; (3) MI-Matrigel group, a total of 150 μL of Matrigel-PBS mixed liquid with a volume ratio of 1:1 supplemented with 5 μM Y27632 was injected to the border area of left ventricle after MI; (4) MI-iPSC-CMs^{modLuc} group, a total of 150 μL of Matrigel and modLuc-transfected iPSC-CMs mixture (5×10^6 cells per rat) with 5 μM Y27632 was injected to the border area of LV after MI; (5) MI-iPSC-CMs^{modVEGF} group, myocardial injection of 150 μL of Matrigel and modVEGF-transfected iPSC-CMs (5×10^6 per rat) mixture with 5 μM Y27632 was performed at the border area of left ventricle after MI. A total of 43 rats were used in this study. Rat model of MI was operated according to the published methods.[41] In addition, we had the CMs transplanted into the recipient hearts immediately after differentiation and transfection rather than undergoing cell freezing and thawing to minimize the impact of cryopreservation and maintain cell viability activity to the greatest extent. In general, rats were placed on the operating table and were subject to endotracheal intubation and continuous anesthesia with isoflurane. After the heart was exposed by left thoracotomy, the permanent ligation of the left anterior descending coronary arteries was then performed with 6-0 sutures to induce MI. For the rats receiving treatments, the exposed hearts received direct myocardial injections of solution or cells at three fixed sites of the infarct border zone as indicated above. Afterward, the chest was closed, and the isoflurane anesthesia was gradually weaned for animal recovery. To avoid immune rejection, 0.25 mg/kg/day tacrolimus and 5 mg/kg/day methylprednisolone were applied as immunosuppressant drugs and given to all the rats every 12 h on the day before MI surgery until 28 days after the MI surgery.

Triphenyl tetrazolium chloride staining

Triphenyl tetrazolium chloride (TTC) staining was performed to delineate the region of MI, which means ischemic areas become colorless while viable heart tissue remains red. Two percent TTC (w/v %) was prepared with PBS and fully dissolved for 30 min at 37°C without light. When rats were sacrificed 24 h post MI, their hearts were collected, washed thoroughly, frozen at −20°C, and sectioned into six 3-mm-thick heart slices. Prewarmed 2% TTC solution was used to stain the heart slices for 30 min at 37°C in the dark. After washing with prewarmed PBS three times, heart slices were fixed with prewarmed 4% PFA for 30 min at 37°C. Photos were taken with a black background and ImageJ was used to analyze the percentage of the infarct area in the left ventricle.

Echocardiography

Echocardiography was performed at 1, 2, and 4 weeks after MI surgery to evaluate the heart function and compare the outcomes of each group. Under inhaled isoflurane anesthesia, rats underwent transthoracic echocardiogram examinations by a blinded technician. The Vevo 2100 Imaging System (VisualSonics) equipped with a 21 MHz MS-250 transducer was applied to observe the LV systolic and diastolic movement. M-mode echocardiographic recordings from a parasternal long-axis view were obtained to measure the LV internal diameter at end-systole (LVIDs) and the LV internal diameter at end-diastole (LVIDd), whereas the LV end-systolic volume (LVESV) and the LV end-diastolic volume (LVEDV) were automatically calculated by the computer software. Heart function indexes, including the LVEF and the LVFS, were finally calculated with the following equations:

$$\text{LVEF (\%)} = ((\text{LVEDV-LVESV})/\text{LVEDV}) \times 100\%$$

$$\text{LVFS (\%)} = ((\text{LVIDd-LVIDs})/\text{LVIDd}) \times 100\%$$

Heart morphology and histological evaluation

Rat hearts were harvested at 1 and 4 weeks post MI. The hearts were fixed in 4% PFA overnight, dehydrated with gradient aqueous ethanol, embedded in paraffin, and then sectioned every 500 μm from the left apex toward the ligation site. After hydration by xylene and a series of graded ethanol solutions, tissue slices were prepared for hematoxylin-eosin staining (Solarbio, China) and Masson trichrome staining (Solarbio, China) according to manufacturers' instructions. Heart morphology was captured with a Leica DM6000 B Microscope. LV wall thickness and scar tissue (%) in left ventricles were calculated under Image-pro plus 6.0.

For immunohistochemistry, microwave antigen retrieval was performed on the hydrated heart slices in citric acid buffer (pH = 6.0) (Yeasen). Heart sections were permeabilized with 0.2% Triton X-100 for 20 min and blocked with 10% goat serum for 1 h at RT. The target proteins were labeled with the primary antibodies at 4°C overnight and then stained with the Alexa Fluor 488/555 conjugated secondary antibodies for 2 h at RT, after which 1:1,000 DAPI (Yeasen) was used to stain nuclei at RT for 10 min. The primary antibodies were provided as follows: Ki67 (ab16667, Abcam), CD31 (ab182981, Abcam), Lamin A + C (ab108595 or ab40567, Abcam), Cx43 (ab11370, Abcam), α-SMA (A5228, Sigma), α-actinin (A7811, Sigma), MLC2v (ab79935, Abcam), cTnT (ab8295, Abcam), CD3 (ab16669, Abcam), and CD68 (ab955, Abcam). The secondary

antibodies consisted of Alexa Fluor 555 conjugated Donkey Anti-Mouse IgG H&L (1:1,000, ab150106, Abcam) and Alexa Fluor 488 conjugated Donkey Anti-Rabbit IgG H&L (1:1,000, ab150073, Abcam). Confocal Laser Scanning Microscope (Leica TSC SP8) was applied for image record and data analysis.

Statistical analysis

Results are expressed as mean ± SD. Differences between groups were evaluated using one-way analyses of variance followed by Bonferroni post test (SPSS, Chicago, IL, USA). All tests were two sided, with a significance level of $p < 0.05$.

SUPPLEMENTAL INFORMATION

Supplemental information can be found online at https://doi.org/10.1016/j.ymthe.2022.08.012.

ACKNOWLEDGMENTS

This work was supported by National Natural Science Foundation of China (82070430), Shanghai Natural Science Foundation (20ZR1434500), the Biomedical Engineering fund of Shanghai Jiao Tong University (YG2021GD04), Science and Technology Development Foundation of Shanghai Pudong (PKJ2020-Y06), and the National Key R&D Program of China (2019YFA0110400). All animal experiments were approved by the Laboratory Animal Welfare Ethics Committee of the Shanghai Children's Medical Center (approval no. SCMC-LAWEC-2019-009).

AUTHOR CONTRIBUTIONS

N.W., K.R.C., and W.F. conceived the idea. X.A., B.Y., N.W., W.W., and W.F. designed the studies. X.A. and B.Y. performed and analyzed the data for most of the experiments. Y.G., L.Y., Y.T., Y.C., M.L., T.L., R.L., and H.W. assisted with performing experiments and analyzing data. X.A., B.Y., N.W., K.R.C., W.W., and W.F. wrote the manuscript with the approval of all other authors.

DECLARATION OF INTERESTS

The authors declare no competing interests.

REFERENCES

1. Zhao, D., Liu, J., Wang, M., Zhang, X., and Zhou, M. (2019). Epidemiology of cardiovascular disease in China: current features and implications. Nat. Rev. Cardiol. *16*, 203–212.
2. Ghostine, S., Carrion, C., Souza, L.C.G., Richard, P., Bruneval, P., Vilquin, J.-T., Pouzet, B., Schwartz, K., Menasché, P., and Hagège, A.A. (2002). Long-term efficacy of myoblast transplantation on regional structure and function after myocardial infarction. Circulation *106*, I131–I136.
3. Silva, G.V., Litovsky, S., Assad, J.A.R., Sousa, A.L.S., Martin, B.J., Vela, D., Coulter, S.C., Lin, J., Ober, J., Vaughn, W.K., et al. (2005). Mesenchymal stem cells differentiate into an endothelial phenotype, enhance vascular density, and improve heart function in a canine chronic ischemia model. Circulation *111*, 150–156.
4. Luo, L., Tang, J., Nishi, K., Yan, C., Dinh, P.-U., Cores, J., Kudo, T., Zhang, J., Li, T.S., and Cheng, K. (2017). Fabrication of synthetic mesenchymal stem cells for the treatment of acute myocardial infarction in mice. Circ. Res. *120*, 1768–1775.
5. Cho, J., Zhai, P., Maejima, Y., and Sadoshima, J. (2011). Myocardial injection with GSK-3β-overexpressing bone marrow-derived mesenchymal stem cells attenuates cardiac dysfunction after myocardial infarction. Circ. Res. *108*, 478–489.
6. Deb, A., Wang, S., Skelding, K.A., Miller, D., Simper, D., and Caplice, N.M. (2003). Bone marrow-derived cardiomyocytes are present in adult human heart: a study of gender-mismatched bone marrow transplantation patients. Circulation *107*, 1247–1249.
7. Sürder, D., Manka, R., Moccetti, T., Lo Cicero, V., Emmert, M.Y., Klersy, C., Soncin, S., Turchetto, L., Radrizzani, M., Zuber, M., et al. (2016). Effect of bone marrow-derived mononuclear cell treatment, early or late after acute myocardial infarction: twelve months CMR and long-term clinical results. Circ. Res. *119*, 481–490.
8. Mathur, A., Fernández-Avilés, F., Bartunek, J., Belmans, A., Crea, F., Dowlut, S., Galiñanes, M., Good, M.C., Hartikainen, J., Hauskeller, C., et al. (2020). The effect of intracoronary infusion of bone marrow-derived mononuclear cells on all-cause mortality in acute myocardial infarction: the BAMI trial. Eur. Heart J. *41*, 3702–3710.
9. Asahara, T., Kawamoto, A., and Masuda, H. (2011). Concise review: circulating endothelial progenitor cells for vascular medicine. Stem cells (Dayton, Ohio) *29*, 1650–1655.
10. Chow, A., Stuckey, D.J., Kidher, E., Rocco, M., Jabbour, R.J., Mansfield, C.A., Darzi, A., Harding, S.E., Stevens, M.M., and Athanasiou, T. (2017). Human induced pluripotent stem cell-derived cardiomyocyte encapsulating bioactive hydrogels improve rat heart function post myocardial infarction. Stem Cel. Rep. *9*, 1415–1422.
11. Funakoshi, S., Fernandes, I., Mastikhina, O., Wilkinson, D., Tran, T., Dhahri, W., Mazine, A., Yang, D., Burnett, B., Lee, J., et al. (2021). Generation of mature compact ventricular cardiomyocytes from human pluripotent stem cells. Nat. Commun. *12*, 3155.
12. Dhahri, W., Sadikov Valdman, T., Wilkinson, D., Pereira, E., Ceylan, E., Andharia, N., Qiang, B., Masoudpour, H., Wulkan, F., Quesnel, E., et al. (2022). In vitro matured human pluripotent stem cell-derived cardiomyocytes form grafts with enhanced structure and function in injured hearts. Circulation *145*, 1412–1426.
13. Shiba, Y., Gomibuchi, T., Seto, T., Wada, Y., Ichimura, H., Tanaka, Y., Ogasawara, T., Okada, K., Shiba, N., Sakamoto, K., et al. (2016). Allogeneic transplantation of iPS cell-derived cardiomyocytes regenerates primate hearts. Nature *538*, 388–391.
14. Laflamme, M.A., Chen, K.Y., Naumova, A.V., Muskheli, V., Fugate, J.A., Dupras, S.K., Reinecke, H., Xu, C., Hassanipour, M., Police, S., et al. (2007). Cardiomyocytes derived from human embryonic stem cells in pro-survival factors enhance function of infarcted rat hearts. Nat. Biotechnol. *25*, 1015–1024.
15. Chong, J.J.H., Yang, X., Don, C.W., Minami, E., Liu, Y.-W., Weyers, J.J., Mahoney, W.M., Van Biber, B., Cook, S.M., Palpant, N.J., et al. (2014). Human embryonic-stem-cell-derived cardiomyocytes regenerate non-human primate hearts. Nature *510*, 273–277.
16. Sheikh, A.Y., Lin, S.-A., Cao, F., Cao, Y., van der Bogt, K.E.A., Chu, P., Chang, C.P., Contag, C.H., Robbins, R.C., and Wu, J.C. (2007). Molecular imaging of bone marrow mononuclear cell homing and engraftment in ischemic myocardium. Stem cells *25*, 2677–2684.
17. Choe, G., Kim, S.-W., Park, J., Park, J., Kim, S., Kim, Y.S., Ahn, Y., Jung, D.W., Williams, D.R., and Lee, J.Y. (2019). Anti-oxidant activity reinforced reduced graphene oxide/alginate microgels: mesenchymal stem cell encapsulation and regeneration of infarcted hearts. Biomaterials *225*, 119513.
18. Chang, C.Y., Chan, A.T., Armstrong, P.A., Luo, H.-C., Higuchi, T., Strehin, I.A., Vakrou, S., Lin, X., Brown, S.N., O'Rourke, B., et al. (2012). Hyaluronic acid-human blood hydrogels for stem cell transplantation. Biomaterials *33*, 8026–8033.
19. Matsumoto, R., Omura, T., Yoshiyama, M., Hayashi, T., Inamoto, S., Koh, K.-R., Ohta, K., Izumi, Y., Nakamura, Y., Akioka, K., et al. (2005). Vascular endothelial growth factor-expressing mesenchymal stem cell transplantation for the treatment of acute myocardial infarction. Arterioscler. Thromb. Vasc. Biol. *25*, 1168–1173.
20. Zimmermann, W.H., Melnychenko, I., Wasmeier, G., Didié, M., Naito, H., Nixdorff, U., Hess, A., Budinsky, L., Brune, K., Michaelis, B., et al. (2006). Engineered heart tissue grafts improve systolic and diastolic function in infarcted rat hearts. Nat. Med. *12*, 452–458.
21. Tiburcy, M., Hudson, J.E., Balfanz, P., Schlick, S., Meyer, T., Chang Liao, M.-L., Levent, E., Raad, F., Zeidler, S., Wingender, E., et al. (2017). Defined engineered human myocardium with advanced maturation for applications in heart failure modeling and repair. Circulation *135*, 1832–1847.
22. Suzuki, K., Murtuza, B., Beauchamp, J.R., Brand, N.J., Barton, P.J.R., Varela-Carver, A., Fukushima, S., Coppen, S.R., Partridge, T.A., and Yacoub, M.H. (2004). Role of

interleukin-1beta in acute inflammation and graft death after cell transplantation to the heart. Circulation *110*, II219–II224.

23. Murtuza, B., Suzuki, K., Bou-Gharios, G., Beauchamp, J.R., Smolenski, R.T., Partridge, T.A., and Yacoub, M.H. (2004). Transplantation of skeletal myoblasts secreting an IL-1 inhibitor modulates adverse remodeling in infarcted murine myocardium. Proc. Natl. Acad. Sci. USA *101*, 4216–4221.
24. Robey, T.E., Saiget, M.K., Reinecke, H., and Murry, C.E. (2008). Systems approaches to preventing transplanted cell death in cardiac repair. J. Mol. Cell. Cardiol. *45*, 567–581.
25. Abdelwahid, E., Kalvelyte, A., Stulpinas, A., de Carvalho, K.A.T., Guarita-Souza, L.C., and Foldes, G. (2016). Stem cell death and survival in heart regeneration and repair. Apoptosis. *21*, 252–268.
26. Tilkorn, D.J., Davies, E.M., Keramidaris, E., Dingle, A.M., Gerrand, Y.-W., Taylor, C.J., Han, X.L., Palmer, J.A., Penington, A.J., Mitchell, C.A., et al. (2012). The in vitro preconditioning of myoblasts to enhance subsequent survival in an in vivo tissue engineering chamber model. Biomaterials *33*, 3868–3879.
27. Rubanyi, G.M. (2013). Mechanistic, technical, and clinical perspectives in therapeutic stimulation of coronary collateral development by angiogenic growth factors. Mol. Ther. *21*, 725–738.
28. Zangi, L., Lui, K.O., von Gise, A., Ma, Q., Ebina, W., Ptaszek, L.M., Später, D., Xu, H., Tabebordbar, M., Gorbatov, R., et al. (2013). Modified mRNA directs the fate of heart progenitor cells and induces vascular regeneration after myocardial infarction. Nat. Biotechnol. *31*, 898–907.
29. Carlsson, L., Clarke, J.C., Yen, C., Gregoire, F., Albery, T., Billger, M., Egnell, A.C., Gan, L.M., Jennbacken, K., Johansson, E., et al. (2018). Biocompatible, purified mRNA improves cardiac function after intracardiac injection 1 Week post-myocardial infarction in swine. Mol. Ther. Methods Clin. Dev. *9*, 330–346.
30. Magadum, A., Singh, N., Kurian, A.A., Sharkar, M.T.K., Chepurko, E., and Zangi, L. (2018). Ablation of a single N-glycosylation site in human FSTL 1 induces cardiomyocyte proliferation and cardiac regeneration. Mol. Ther. Nucleic Acids *13*, 133–143.
31. Magadum, A., Singh, N., Kurian, A.A., Munir, I., Mehmood, T., Brown, K., Sharkar, M.T.K., Chepurko, E., Sassi, Y., Oh, J.G., et al. (2020). Pkm2 regulates cardiomyocyte cell cycle and promotes cardiac regeneration. Circulation *141*, 1249–1265.
32. Lin, G., Zhang, H., and Huang, L. (2015). Smart polymeric nanoparticles for cancer gene delivery. Mol. Pharm. *12*, 314–321.
33. Yu, Z., Witman, N., Wang, W., Li, D., Yan, B., Deng, M., Wang, X., Wang, H., Zhou, G., Liu, W., et al. (2019). Cell-mediated delivery of VEGF modified mRNA enhances blood vessel regeneration and ameliorates murine critical limb ischemia. J. Control Release *310*, 103–114.
34. Geng, Y., Duan, H., Xu, L., Witman, N., Yan, B., Yu, Z., Wang, H., Tan, Y., Lin, L., Li, D., et al. (2021). BMP-2 and VEGF-A modRNAs in collagen scaffold synergistically drive bone repair through osteogenic and angiogenic pathways. Commun. Biol. *4*, 82.
35. Lian, X., Zhang, J., Azarin, S.M., Zhu, K., Hazeltine, L.B., Bao, X., Hsiao, C., Kamp, T.J., and Palecek, S.P. (2013). Directed cardiomyocyte differentiation from human pluripotent stem cells by modulating Wnt/β-catenin signaling under fully defined conditions. Nat. Protoc. *8*, 162–175.
36. Gomez-Garcia, M.J., Quesnel, E., Al-Attar, R., Laskary, A.R., and Laflamme, M.A. (2021). Maturation of human pluripotent stem cell derived cardiomyocytes in vitro and in vivo. Semin. Cell Dev. Biol. *118*, 163–171.
37. Reffelmann, T., Dow, J.S., Dai, W., Hale, S.L., Simkhovich, B.Z., and Kloner, R.A. (2003). Transplantation of neonatal cardiomyocytes after permanent coronary artery occlusion increases regional blood flow of infarcted myocardium. J. Mol. Cell. Cardiol. *35*, 607–613.
38. Foo, K.S., Lehtinen, M.L., Leung, C.Y., Lian, X., Xu, J., Keung, W., Geng, L., Kolstad, T.R.S., Thams, S., Wong, A.O.T., et al. (2018). Human ISL1 ventricular progenitors self-assemble into an in vivo functional heart patch and preserve cardiac function post infarction. Mol. Ther. *26*, 1644–1659.
39. Tu, C., and Zoldan, J. (2018). Moving iPSC-derived cardiomyocytes forward to treat myocardial infarction. Cell Stem Cell *23*, 322–323.
40. Caspi, O., Huber, I., Kehat, I., Habib, M., Arbel, G., Gepstein, A., Yankelson, L., Aronson, D., Beyar, R., and Gepstein, L. (2007). Transplantation of human embryonic stem cell-derived cardiomyocytes improves myocardial performance in infarcted rat hearts. J. Am. Coll. Cardiol. *50*, 1884–1893.
41. Murry, C.E., Soonpaa, M.H., Reinecke, H., Nakajima, H., Nakajima, H.O., Rubart, M., Pasumarthi, K.B.S., Virag, J.I., Bartelmez, S.H., Poppa, V., et al. (2004). Haematopoietic stem cells do not transdifferentiate into cardiac myocytes in myocardial infarcts. Nature *428*, 664–668.
42. Shiba, Y., Fernandes, S., Zhu, W.-Z., Filice, D., Muskheli, V., Kim, J., Palpant, N.J., Gantz, J., Moyes, K.W., Reinecke, H., et al. (2012). Human ES-cell-derived cardiomyocytes electrically couple and suppress arrhythmias in injured hearts. Nature *489*, 322–325.
43. Kadota, S., Pabon, L., Reinecke, H., and Murry, C.E. (2017). In vivo maturation of human induced pluripotent stem cell-derived cardiomyocytes in neonatal and adult rat hearts. Stem Cel. Rep. *8*, 278–289.
44. Chen, H.-S.V., Kim, C., and Mercola, M. (2009). Electrophysiological challenges of cell-based myocardial repair. Circulation *120*, 2496–2508.
45. Reinecke, H., Zhang, M., Bartosek, T., and Murry, C.E. (1999). Survival, integration, and differentiation of cardiomyocyte grafts: a study in normal and injured rat hearts. Circulation *100*, 193–202.
46. Wall, S.T., Walker, J.C., Healy, K.E., Ratcliffe, M.B., and Guccione, J.M. (2006). Theoretical impact of the injection of material into the myocardium: a finite element model simulation. Circulation *114*, 2627–2635.
47. Hodgkinson, C.P., Bareja, A., Gomez, J.A., and Dzau, V.J. (2016). Emerging concepts in paracrine mechanisms in regenerative cardiovascular medicine and biology. Circ. Res. *118*, 95–107.
48. Romagnuolo, R., Masoudpour, H., Porta-Sánchez, A., Qiang, B., Barry, J., Laskary, A., Qi, X., Massé, S., Magtibay, K., Kawajiri, H., et al. (2019). Human embryonic stem cell-derived cardiomyocytes regenerate the infarcted pig heart but induce ventricular tachyarrhythmias. Stem Cel. Rep. *12*, 967–981.
49. Zhu, K., Wu, Q., Ni, C., Zhang, P., Zhong, Z., Wu, Y., Wang, Y., Xu, Y., Kong, M., Cheng, H., et al. (2018). Lack of remuscularization following transplantation of human embryonic stem cell-derived cardiovascular progenitor cells in infarcted nonhuman primates. Circ. Res. *122*, 958–969.
50. Tachibana, A., Santoso, M.R., Mahmoudi, M., Shukla, P., Wang, L., Bennett, M., Goldstone, A.B., Wang, M., Fukushi, M., Ebert, A.D., et al. (2017). Paracrine effects of the pluripotent stem cell-derived cardiac myocytes salvage the injured myocardium. Circ. Res. *121*, e22–e36.
51. Ong, S.G., Huber, B.C., Lee, W.H., Kodo, K., Ebert, A.D., Ma, Y., Nguyen, P.K., Diecke, S., Chen, W.Y., and Wu, J.C. (2015). Microfluidic single-cell analysis of transplanted human induced pluripotent stem cell-derived cardiomyocytes after acute myocardial infarction. Circulation *132*, 762–771.
52. Sanchez-Freire, V., Lee, A.S., Hu, S., Abilez, O.J., Liang, P., Lan, F., Huber, B.C., Ong, S.G., Hong, W.X., Huang, M., and Wu, J.C. (2014). Effect of human donor cell source on differentiation and function of cardiac induced pluripotent stem cells. J. Am. Coll. Cardiol. *64*, 436–448.
53. Fernandes, S., Chong, J.J.H., Paige, S.L., Iwata, M., Torok-Storb, B., Keller, G., Reinecke, H., and Murry, C.E. (2015). Comparison of human embryonic stem cell-derived cardiomyocytes, cardiovascular progenitors, and bone marrow mononuclear cells for cardiac repair. Stem Cel. Rep. *5*, 753–762.
54. Hu, X., Xu, Y., Zhong, Z., Wu, Y., Zhao, J., Wang, Y., Cheng, H., Kong, M., Zhang, F., Chen, Q., et al. (2016). A large-scale investigation of hypoxia-preconditioned allogeneic mesenchymal stem cells for myocardial repair in nonhuman primates: paracrine activity without remuscularization. Circ. Res. *118*, 970–983.
55. Ye, L., Chang, Y.H., Xiong, Q., Zhang, P., Zhang, L., Somasundaram, P., Lepley, M., Swingen, C., Su, L., Wendel, J.S., et al. (2014). Cardiac repair in a porcine model of acute myocardial infarction with human induced pluripotent stem cell-derived cardiovascular cells. Cell stem cell *15*, 750–761.
56. Fernandes, S., Naumova, A.V., Zhu, W.Z., Laflamme, M.A., Gold, J., and Murry, C.E. (2010). Human embryonic stem cell-derived cardiomyocytes engraft but do not alter cardiac remodeling after chronic infarction in rats. J. Mol. Cell. Cardiol. *49*, 941–949.
57. Ichimura, H., Kadota, S., Kashihara, T., Yamada, M., Ito, K., Kobayashi, H., Tanaka, Y., Shiba, N., Chuma, S., Tohyama, S., et al. (2020). Increased predominance of the matured ventricular subtype in embryonic stem cell-derived cardiomyocytes in vivo. Sci. Rep. *10*, 11883.

58. Kawamura, M., Miyagawa, S., Fukushima, S., Saito, A., Miki, K., Funakoshi, S., Yoshida, Y., Yamanaka, S., Shimizu, T., Okano, T., et al. (2017). Enhanced therapeutic effects of human iPS cell derived-cardiomyocyte by combined cell-sheets with omental flap technique in porcine ischemic cardiomyopathy model. Sci. Rep. *7*, 8824.

59. Cui, H., Liu, C., Esworthy, T., Huang, Y., Yu, Z.-X., Zhou, X., San, H., Lee, S.J., Hann, S.Y., Boehm, M., et al. (2020). 4D physiologically adaptable cardiac patch: a 4-month in vivo study for the treatment of myocardial infarction. Sci. Adv. *6*, eabb5067.

60. Ou, L., Li, W., Zhang, Y., Wang, W., Liu, J., Sorg, H., Furlani, D., Gäbel, R., Mark, P., Klopsch, C., et al. (2011). Intracardiac injection of matrigel induces stem cell recruitment and improves cardiac functions in a rat myocardial infarction model. J. Cell. Mol. Med. *15*, 1310–1318.

61. Braile, M., Marcella, S., Cristinziano, L., Galdiero, M.R., Modestino, L., Ferrara, A.L., Varricchi, G., Marone, G., and Loffredo, S. (2020). VEGF-A in cardiomyocytes and heart diseases. Int. J. Mol. Sci. *21*, E5294.

62. Gilmore, T., Gapuzan, M.-E., Kalaitzidis, D., and Starczynowski, D. (2002). Rel/NF-kappa B/I kappa B signal transduction in the generation and treatment of human cancer. Cancer Lett. *181*, 1–9.

63. Szabo, C. (2016). Gasotransmitters in cancer: from pathophysiology to experimental therapy. Nat. Rev. Drug Discov. *15*, 185–203.

64. Yadav, A.K., Renfrow, J.J., Scholtens, D.M., Xie, H., Duran, G.E., Bredel, C., Vogel, H., Chandler, J.P., Chakravarti, A., Robe, P.A., et al. (2009). Monosomy of chromosome 10 associated with dysregulation of epidermal growth factor signaling in glioblastomas. JAMA *302*, 276–289.

65. Boomer, J.S., and Green, J.M. (2010). An enigmatic tail of CD28 signaling. Cold Spring Harb. Perspect. Biol. *2*, a002436.

66. Karra, R., Foglia, M.J., Choi, W.-Y., Belliveau, C., DeBenedittis, P., and Poss, K.D. (2018). Vegfaa instructs cardiac muscle hyperplasia in adult zebrafish. Proc. Natl. Acad. Sci. USA *115*, 8805–8810.

67. Locatelli, P., Olea, F.D., Hnatiuk, A., De Lorenzi, A., Cerdá, M., Giménez, C.S., Sepúlveda, D., Laguens, R., and Crottogini, A. (2015). Mesenchymal stromal cells overexpressing vascular endothelial growth factor in ovine myocardial infarction. Gene Ther. *22*, 449–457.

68. Giacomelli, E., Meraviglia, V., Campostrini, G., Cochrane, A., Cao, X., van Helden, R.W.J., Krotenberg Garcia, A., Mircea, M., Kostidis, S., Davis, R.P., et al. (2020). Human-iPSC-Derived cardiac stromal cells enhance maturation in 3D cardiac microtissues and reveal non-cardiomyocyte contributions to heart disease. Cell stem cell *26*, 862–879.e11. e811.

69. Dor, Y., Djonov, V., Abramovitch, R., Itin, A., Fishman, G.I., Carmeliet, P., Goelman, G., and Keshet, E. (2002). Conditional switching of VEGF provides new insights into adult neovascularization and pro-angiogenic therapy. EMBO J. *21*, 1939–1947.

70. Lee, R.J., Springer, M.L., Blanco-Bose, W.E., Shaw, R., Ursell, P.C., and Blau, H.M. (2000). VEGF gene delivery to myocardium: deleterious effects of unregulated expression. Circulation *102*, 898–901.

71. Gong, Y., Chen, Z., Yang, L., Ai, X., Yan, B., Wang, H., Qiu, L., Tan, Y., Witman, N., Wang, W., et al. (2020). Intrinsic color sensing system Allows for real-time observable functional changes on human induced pluripotent stem cell-derived cardiomyocytes. ACS Nano *14*, 8232–8246.

YMTHE, Volume *31*

Supplemental Information

Transient secretion of VEGF protein from transplanted hiPSC-CMs enhances engraftment and improves rat heart function post MI

Xuefeng Ai, Bingqian Yan, Nevin Witman, Yiqi Gong, Li Yang, Yao Tan, Ying Chen, Minglu Liu, Tingting Lu, Runjiao Luo, Huijing Wang, Kenneth R. Chien, Wei Wang, and Wei Fu

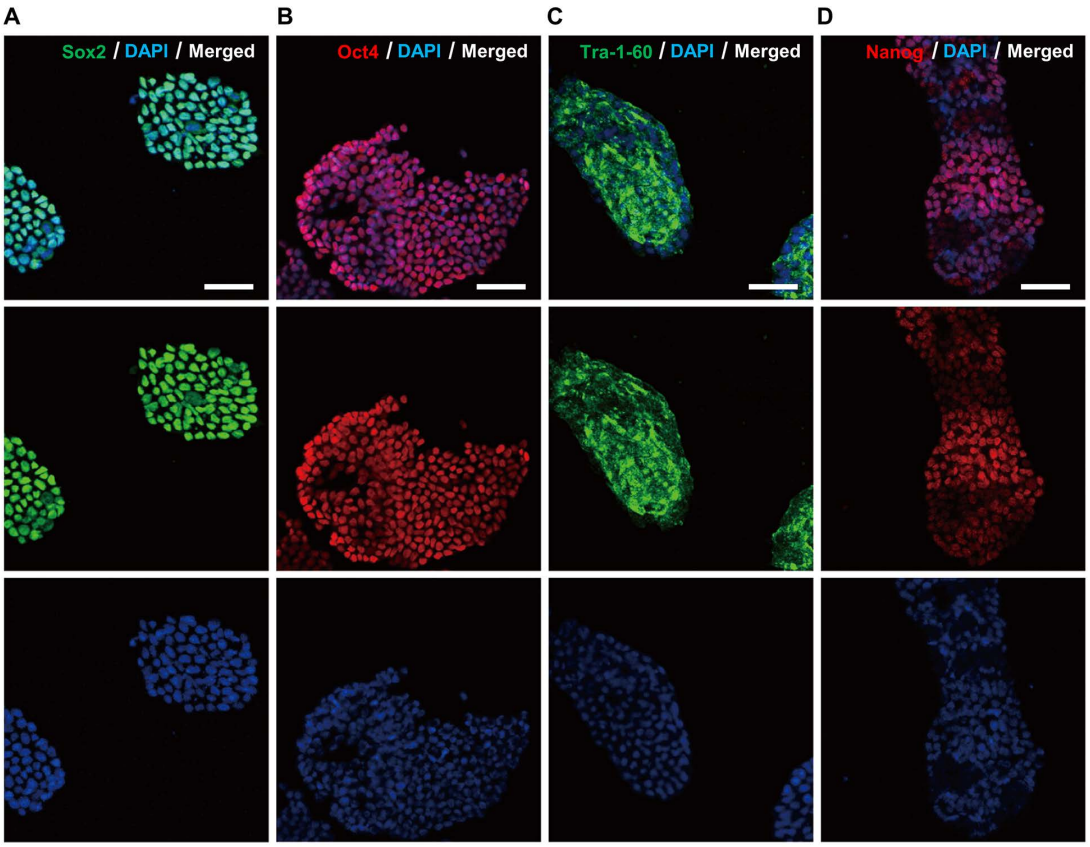

Figure S1. Representative immunohistochemistry staining of iPSCs expressing pluripotency markers.

(A-D) Representative immunostainings of iPSCs expressing Sox2 (A), Oct4 (B), TRA-1-60 (C), and Nanog (D). Scale bar, 25μm.

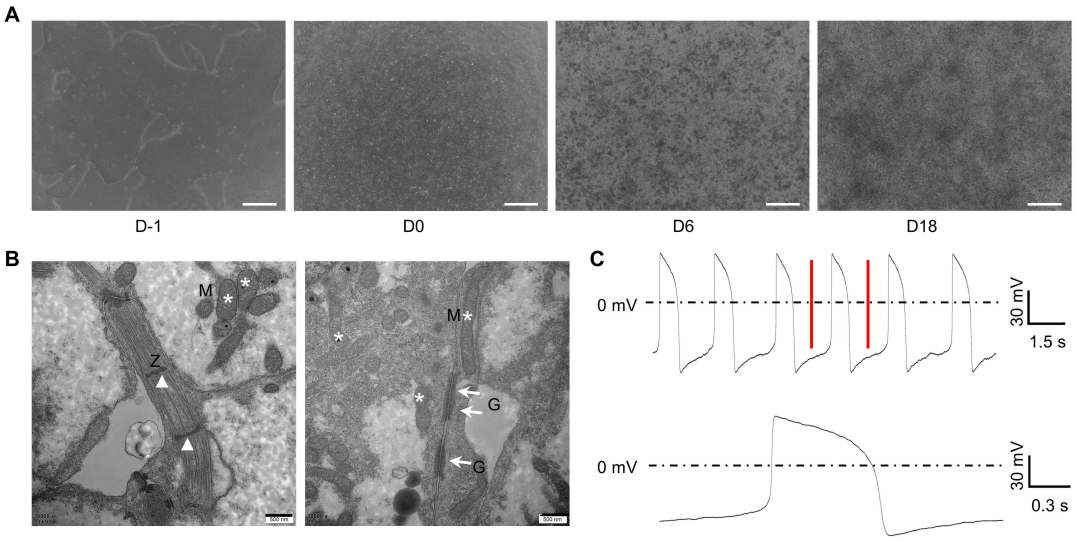

Figure S2. Characteristics of differentiating iPSCs and iPSC-derived cardiomyocytes (iPSC-CMs)

(A) Representative images of iPSCs before the start of differentiation and at several stages after initiation of cardiac differentiation. Scale bar, 500nm. (B) Transmission electron microscope of iPSC-CMs reveal structural details of the sarcomere, Z-line, mitochondria, and gap junctions. Z, white arrowhead indicates Z line; M, white asterisk indicates mitochondria; G, white arrows indicate gap junction. Scale bar, 500nm. (C) Patch clamp recordings showcase action potentials of a single cardiomyocyte. A single action potential magnifies the waveform. The dotted line indicates that the resting potential at 0 mV.

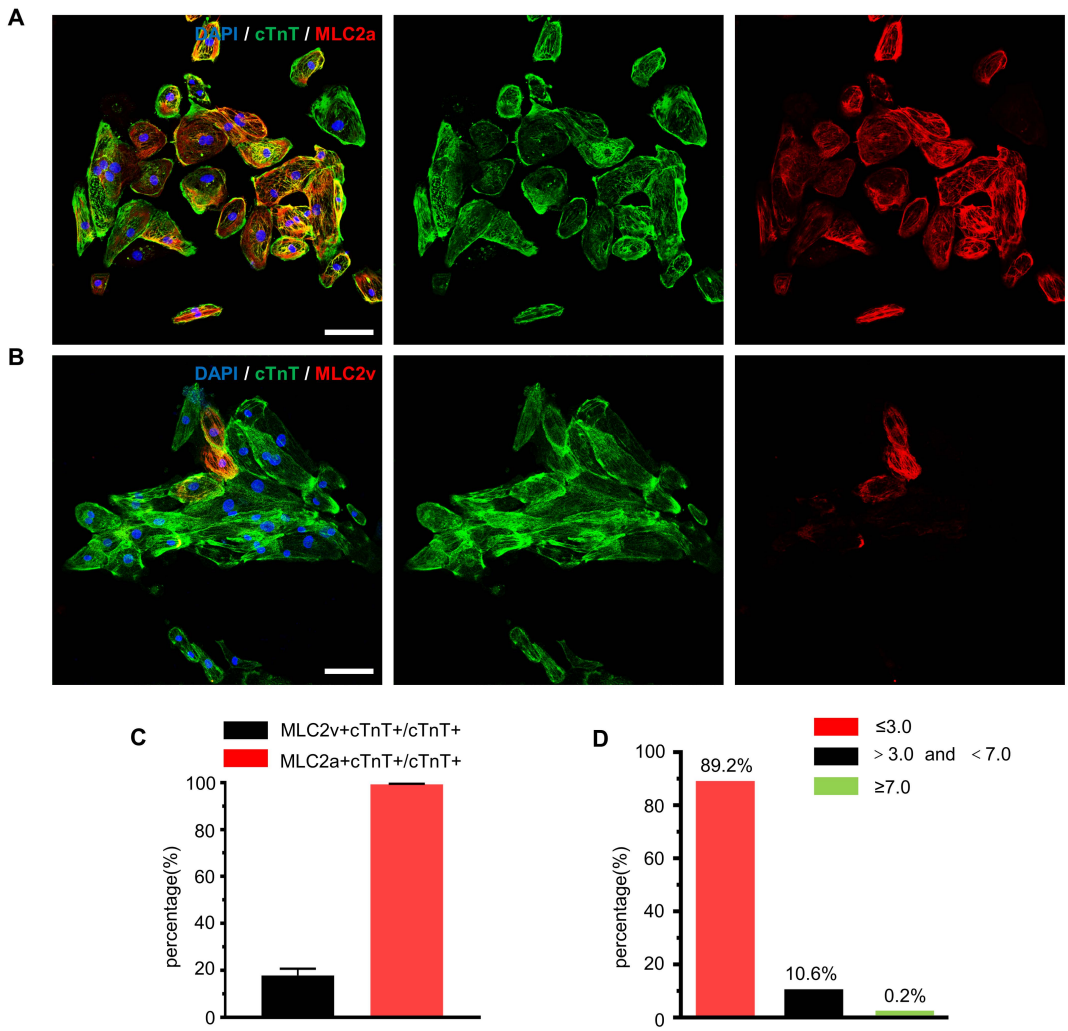

Figure S3. Cardiomyocyte maturation on day 18 of differentiation

(A-B) Representative immunofluorescent images of cardiomyocytes on day 18 of differentiation stained with myocardial structural markers cTnT, MLC2a and MLC2v. A, green, cTnT; red, MLC2a; blue, DAPI; B, green, cTnT; red, MLC2v; blue, DAPI. (Scale bar=75μm). (C) Quantitative analysis of the ratio of MLC2a+cTnT+/cTnT+ and MLC2v+cTnT+/cTnT+ cardiomyocytes. (n=5). (D) Quantitative analysis of the ratio of cardiomyocyte length to width.

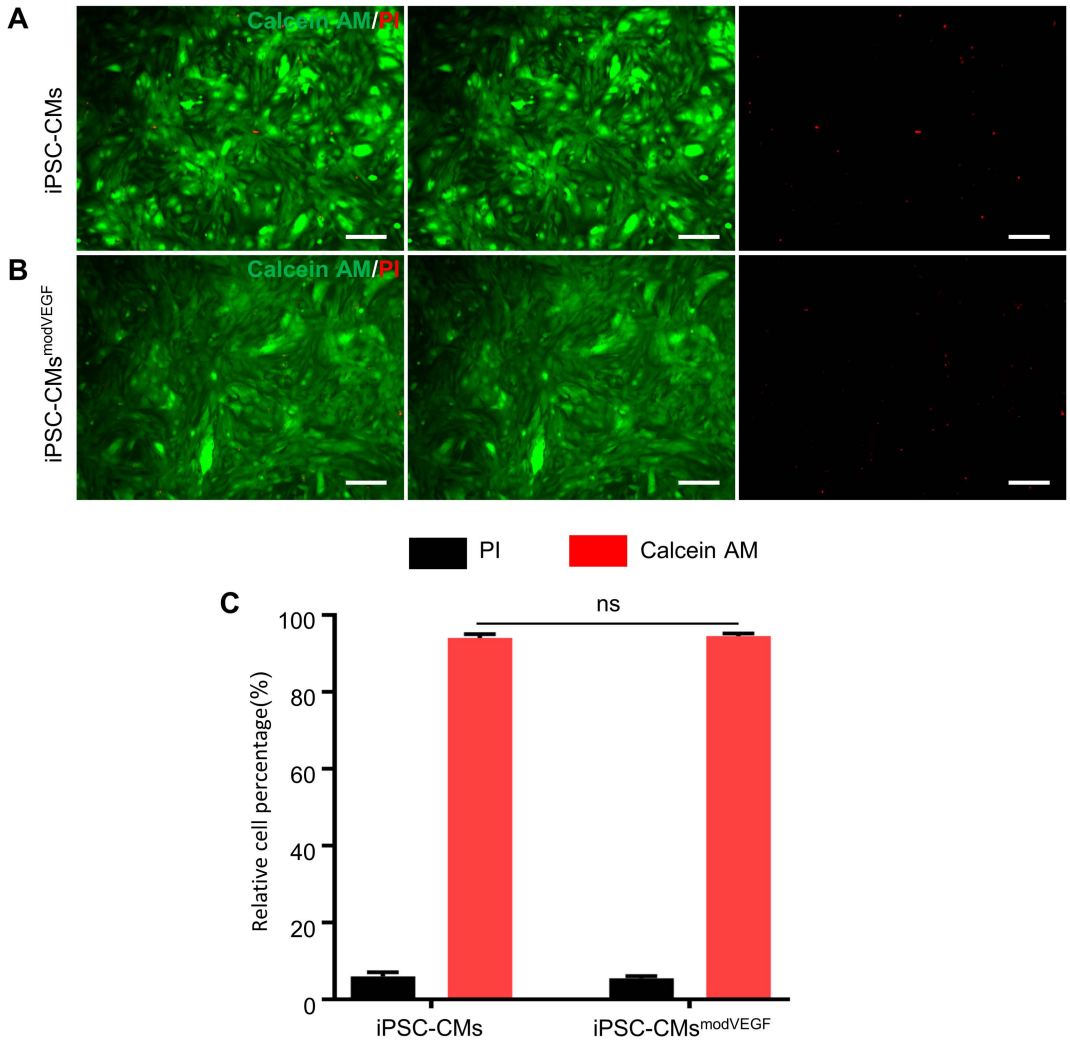

Figure S4. Viability of iPSC-CMs following modRNA transfection

(A-B) Live/dead cell staining 24 hours post-transfection with modRNA: green, Calcein AM, live cells; red, PI, dead cells, Scale bar=150 μm. (C) Quantitative analysis of the ratio of live/dead cells following transfection. (n=5). P values were determined by one-way analyses of variance followed by Bonferroni post-test. (ns indicates $P > 0.05$).

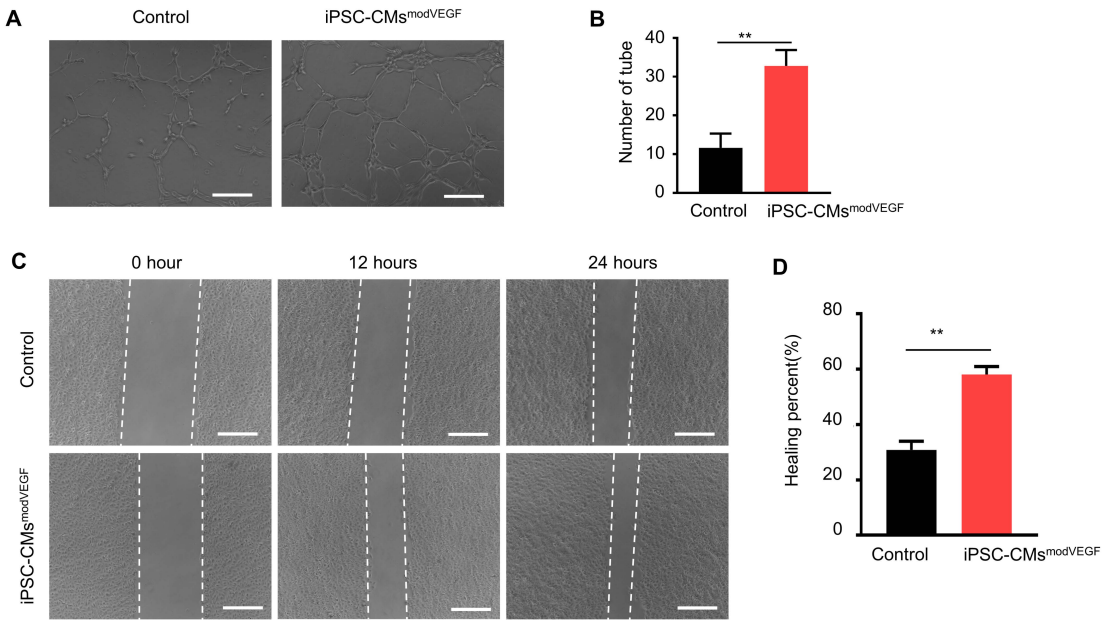

Figure S5. Cell culture supernatant from VEGF-mRNA transfected iPSC-CMs promote functional angiogenic properties

(A) Representative photomicrographs of the tubule formation assay on cultured human umbilical vein endothelial cells (HUVEC), following media changes and (B) quantitative analysis of the number of tubules formed (5 biological repeats for each group). Scale bar=500 μm. (C) Scratch wound healing assay of HUVECs treated with serum lysates from either non-transfected iPSC-CMs (control) or iPSC-CMs transfected with VEGF modRNA and analyzed at 0, 12, 24 hours. Scale bar=500 μm. (D) Quantitative analysis of 24-hour scratch healing rate (5 biological repeats for each group). P values were determined by one-way analyses of variance followed by Bonferroni post-test. (*p <0.05, **p <0.01).

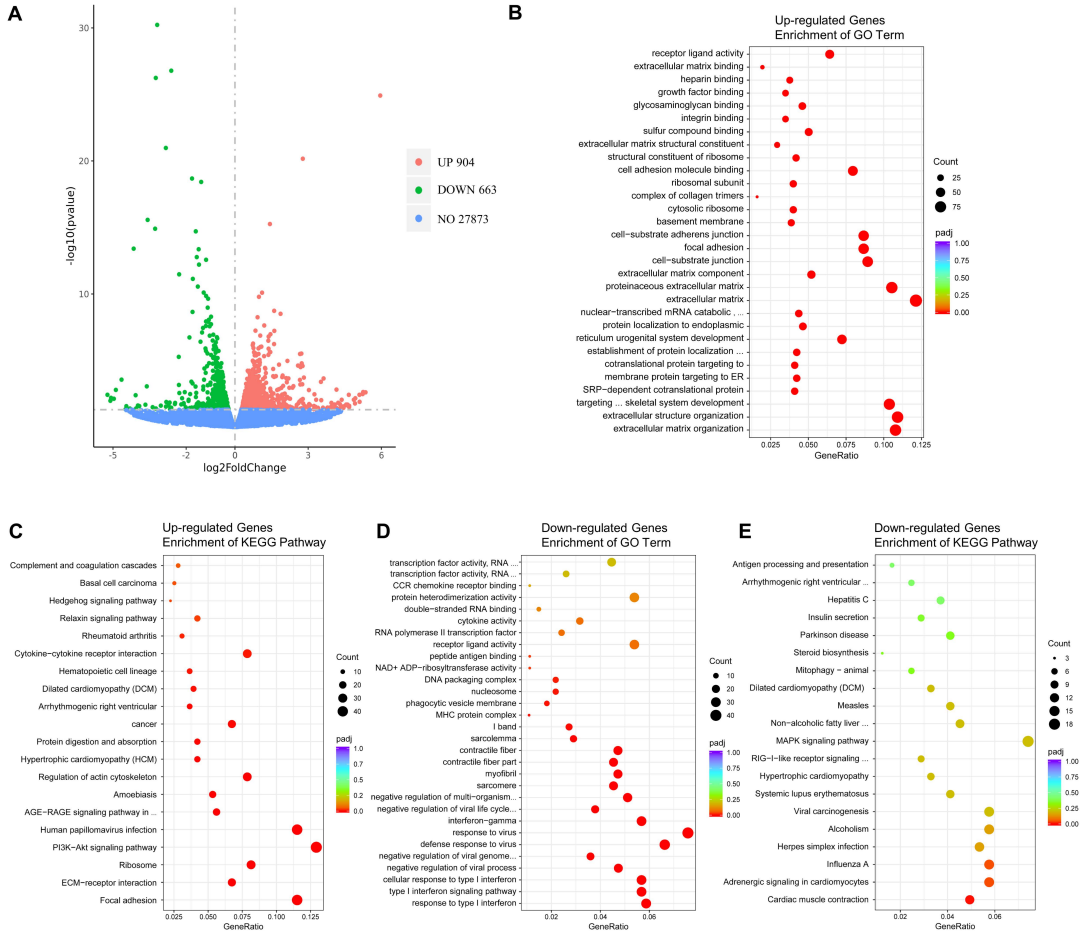

Figure S6. RNA-sequencing data obtained from the modVEGF transfected iPSC-CMs

(A) Volcano plot of all differentially expressed genes on day three post-transfection. UP means up-regulated gene expression, DOWN means down-regulated gene expression, and NO means no differentially expressed gene. (B) GO enrichment analysis of all up-regulated DEGs, and the most significant 30 GO terms were displayed in the bubble chart. The size of the bubble indicates the number of clustered genes, and the color of the bubble indicates the adjusted p-value (padj). (C) KEGG pathway analysis of all up-regulated DEGs, and the bubble chart shows the most significant 20 KEGG pathways. The size of the bubble indicates the number of clustered genes, and the color of the bubble indicates padj. (D) GO enrichment analysis of all down-regulated DEGs, and the bubble chart shows the most significant 30 GO terms. The size of the bubble indicates the number of clustered genes, and the color of the bubble indicates padj. (E)

KEGG pathway analysis of all down-regulated DEGs, and the bubble chart shows the most significant 20 KEGG pathways. The size of the bubble indicates the number of clustered genes, and the color of the bubble indicates padj.

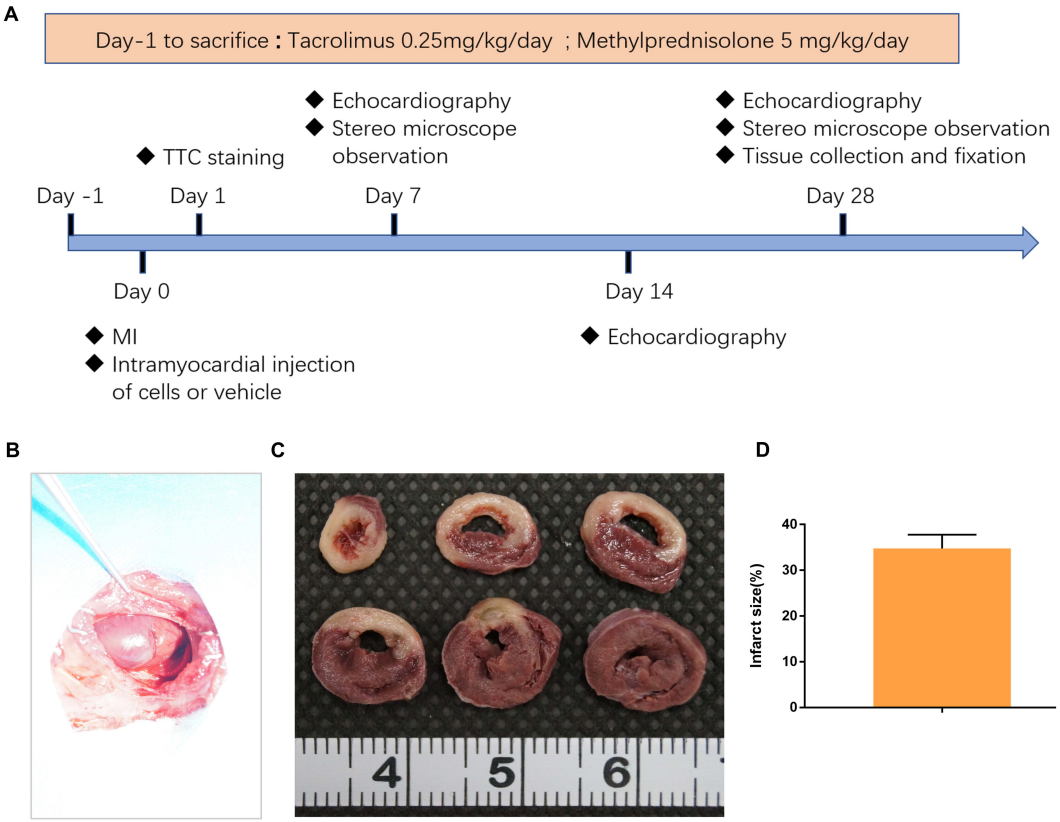

Figure S7. Schematic illustration and overview of the myocardial infarction injury model

(A) Schematic diagram of surgical protocol including in vivo research design and experimental data collection time. (B) Representative image of rat heart after myocardial infarction surgery. (C) Representative TTC staining revealed white ischemic areas where blanching occurred. (D) Comparison of infarcted areas in transversely sectioned hearts at 28 days after the onset of myocardial injury (34.8% ± 2.7%, n = 5; data are means ± SD).

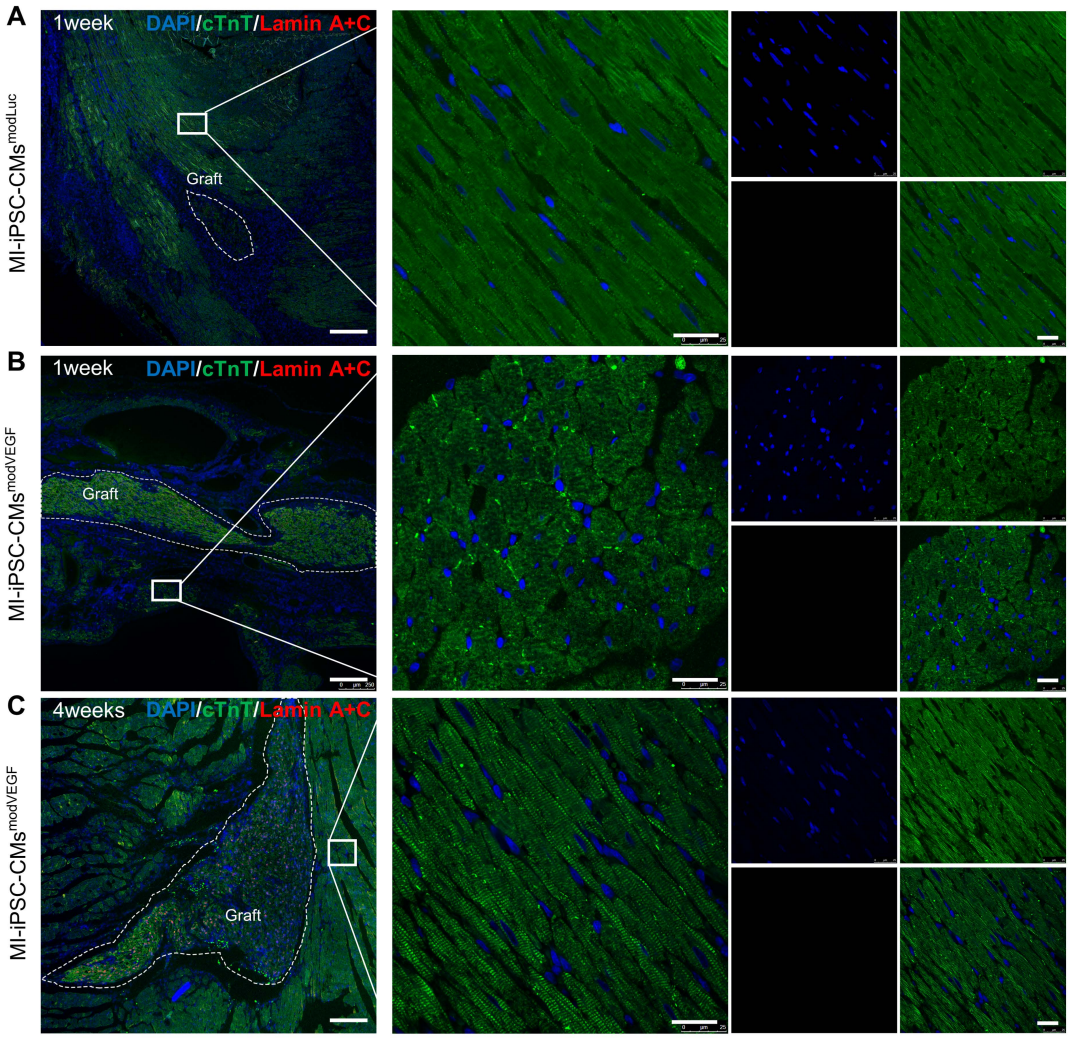

Figure S8. Identification of localized human cardiac muscle islands in the rat myocardium

Representative confocal immunofluorescence images of rat hearts subjected to myocardial infarction and transplantation of iPSC-CMs 1 week (A-B) or 4 weeks (C) after engraftment: green, cTnT; red, Lamin A/C; blue, DAPI. Note: The images in the left panel in Figure S8A-C are reproduced from the left panel images shown in Figure 2B-D to further illustrate the surrounding environments of the engrafted areas. Scale bar on the left: 250 μm. Scale bars (zoomed snapshot): 25 μm.

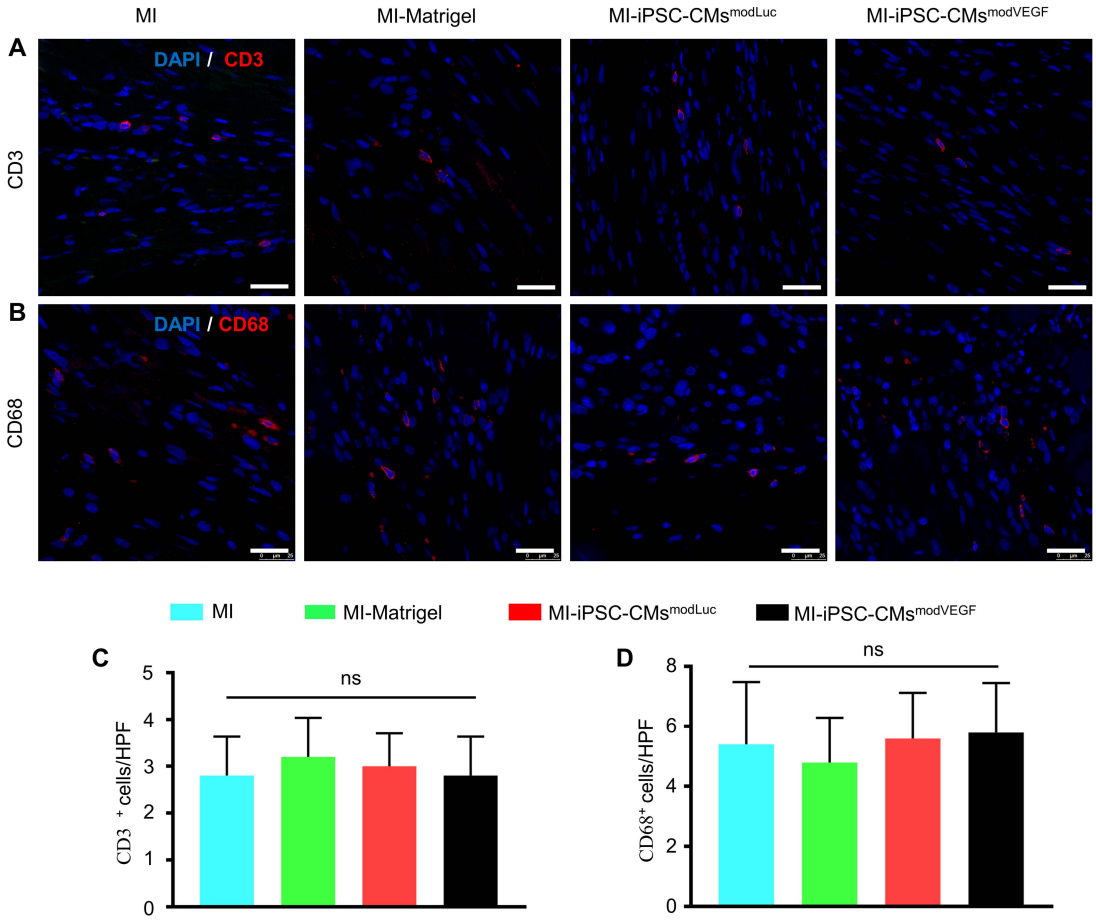

Figure S9. Minimal immune responses after iPSC-CM transplantation

(A-B) Representative confocal images of CD3 and CD68 expression at 4 weeks post-transplantation (scale bar=25 μm). (C) Quantitative analysis of CD3+ immune cell numbers per high powered field (HPF) (n=5). (D) Quantitative analysis of CD68+ immune cell numbers per HPF (n=5). P values were determined by one-way analyses of variance followed by Bonferroni post-test. (ns indicates $P > 0.05$).

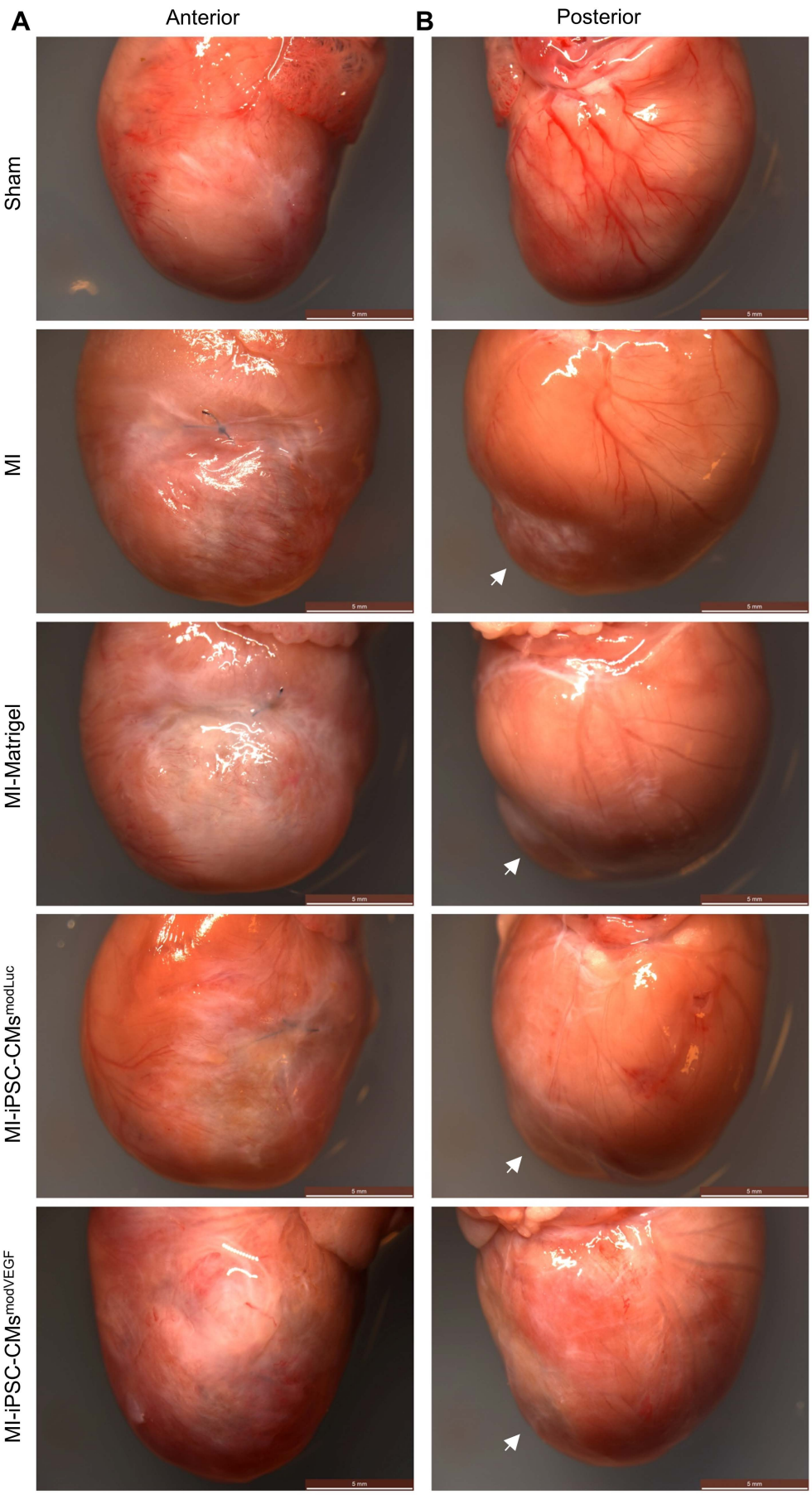
A
Anterior
B
Posterior
Sham
MI
MI-Matrigel
MI-iPSC-CMsmodLuc
MI-iPSC-CMsmodVEGF

Figure S10. Gross morphology of rat heart at 4 weeks after myocardial infarction

Representative digital photographs of whole exposed rat hearts 4 weeks after infarction and iPSC-CMs transplantation, anterior (A) and posterior (B) views. The white arrow indicates the apex from the posterior view.

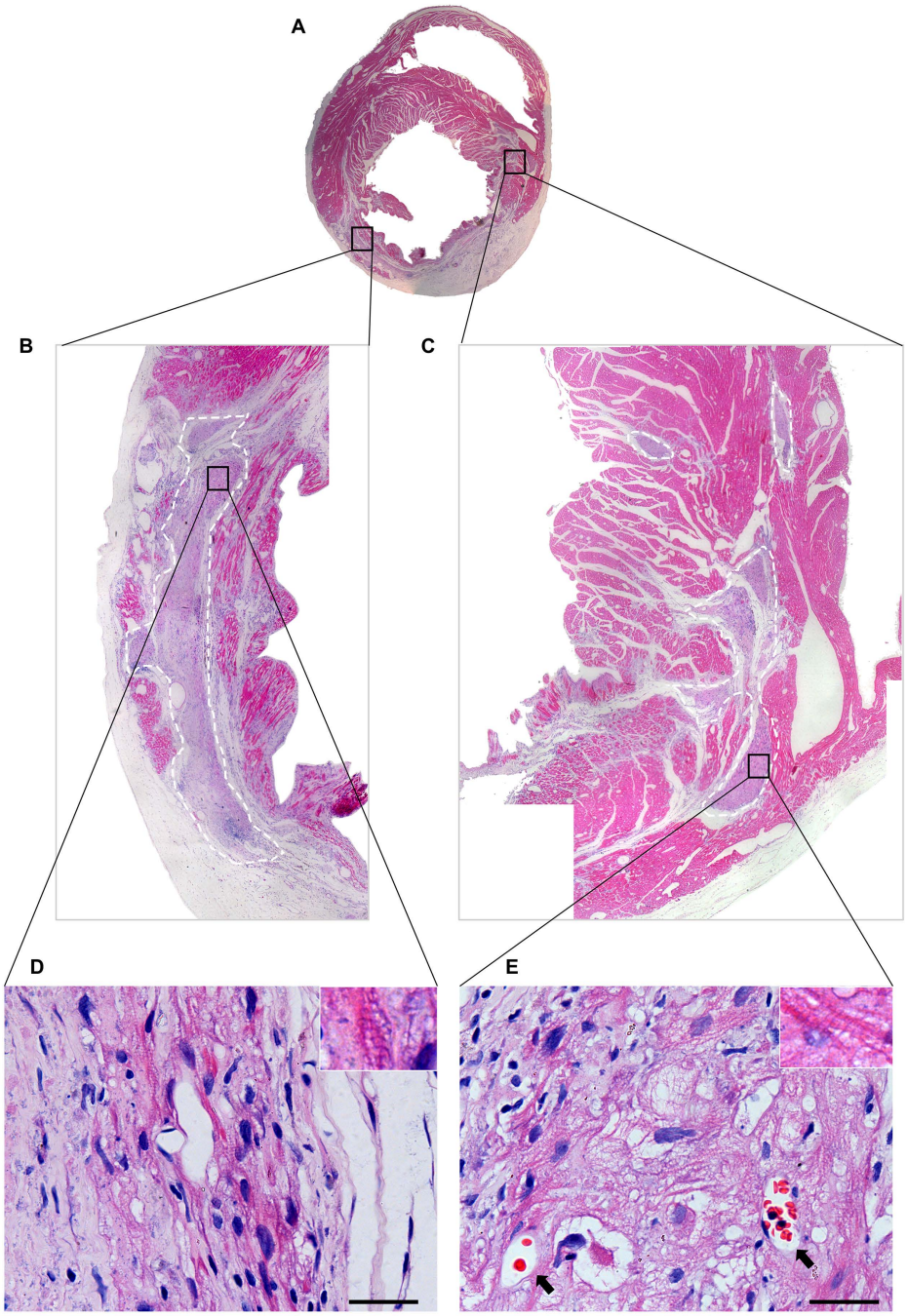

Figure S11. Detection of surviving myocardial grafts in the border zone and infarction zone of the iPSC-CMs^{modVEGF} group at 4 weeks post-transplantation

(A) Representative photograph of a transverse sectioned rat heart receiving iPSC-CMs^{modVEGF} treatment, stained with hematoxylin and eosin. Note: Figure S11A is reproduced from the image in the bottom row in Figure 4A to illustrate improved muscle wall thickness corresponding to areas of high cell-retention. (B-C) Enlarged view of border zone depicting the surviving grafts. (D-E) The high magnification

microscope images reveal that the grafts have complete cell morphology and sarcomeric structure (inset at upper right), black arrows indicate blood vessel in graft. Scale bar, 20μm.

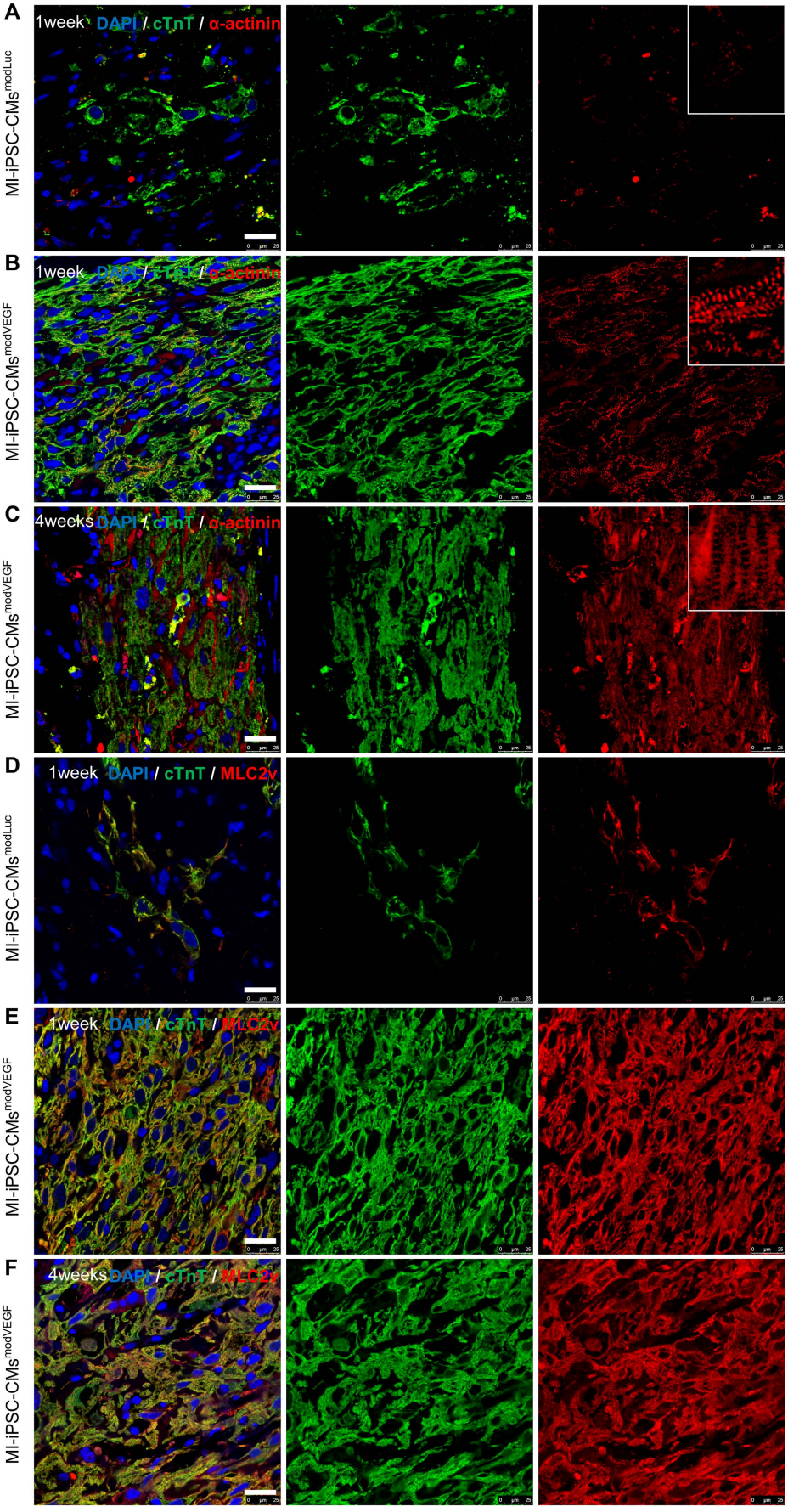
A
1week DAPI / cTnT / α-actinin
MI-iPSC-CMsmodLuc
B
1week DAPI / cTnT / α-actinin
MI-iPSC-CMsmodVEGF
C
4weeks DAPI / cTnT / α-actinin
MI-iPSC-CMsmodVEGF
D
1week DAPI / cTnT / MLC2v
MI-iPSC-CMsmodLuc
E
1week DAPI / cTnT / MLC2v
MI-iPSC-CMsmodVEGF
F
4weeks DAPI / cTnT / MLC2v
MI-iPSC-CMsmodVEGF

Figure S12. Phenotypic profiling of the transplanted and grafted iPSC-CMs

Expression of sarcomeric α-actinin (red) and troponin cTnT (green) in the MI-iPSC-CMs^{modLuc} group (A) and MI-iPSC-CMs^{modVEGF} group (B) 1-week post-transplantation. Scale bar, 25μm. (C) Expression of sarcomeric α-actinin (red) and troponin cTnT (green) in the MI-iPSC-CMs^{modVEGF} group in the grafted region 4 weeks post-transplantation. Scale bar, 25μm. Expression of myosin MLC2v (red) and troponin cTnT (green) in the MI-iPSC-CMs^{modLuc} group (D) and in the MI-iPSC-CMs^{modVEGF} group (E) 1-week post-transplantation. Scale bar, 25μm. (F) Expression of myosin MLC2v (red) and troponin cTnT (green) in the MI-iPSC-CMs^{modVEGF} group in the graft 4 weeks post-transplantation. Scale bar, 25μm.

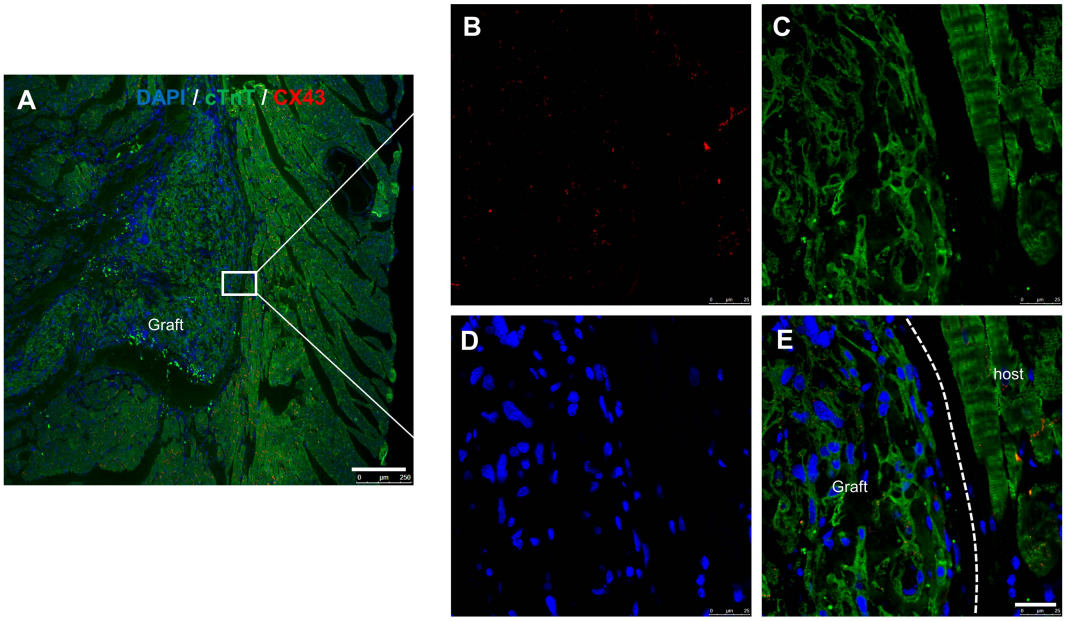

Figure S13. No evidence for gap junction formation between graft and host

(A) Representative confocal pictures of the expression of Cx43 in the myocardial grafts at 4 weeks post-transplantation of iPSC-CMs^{modVEGF}, (scale bar: 250 µm). (B-E) Enlarged view of the border zone between graft and host myocardium, (scale bar: 25 µm), green, cTnT; red, Cx43; blue, DAPI.

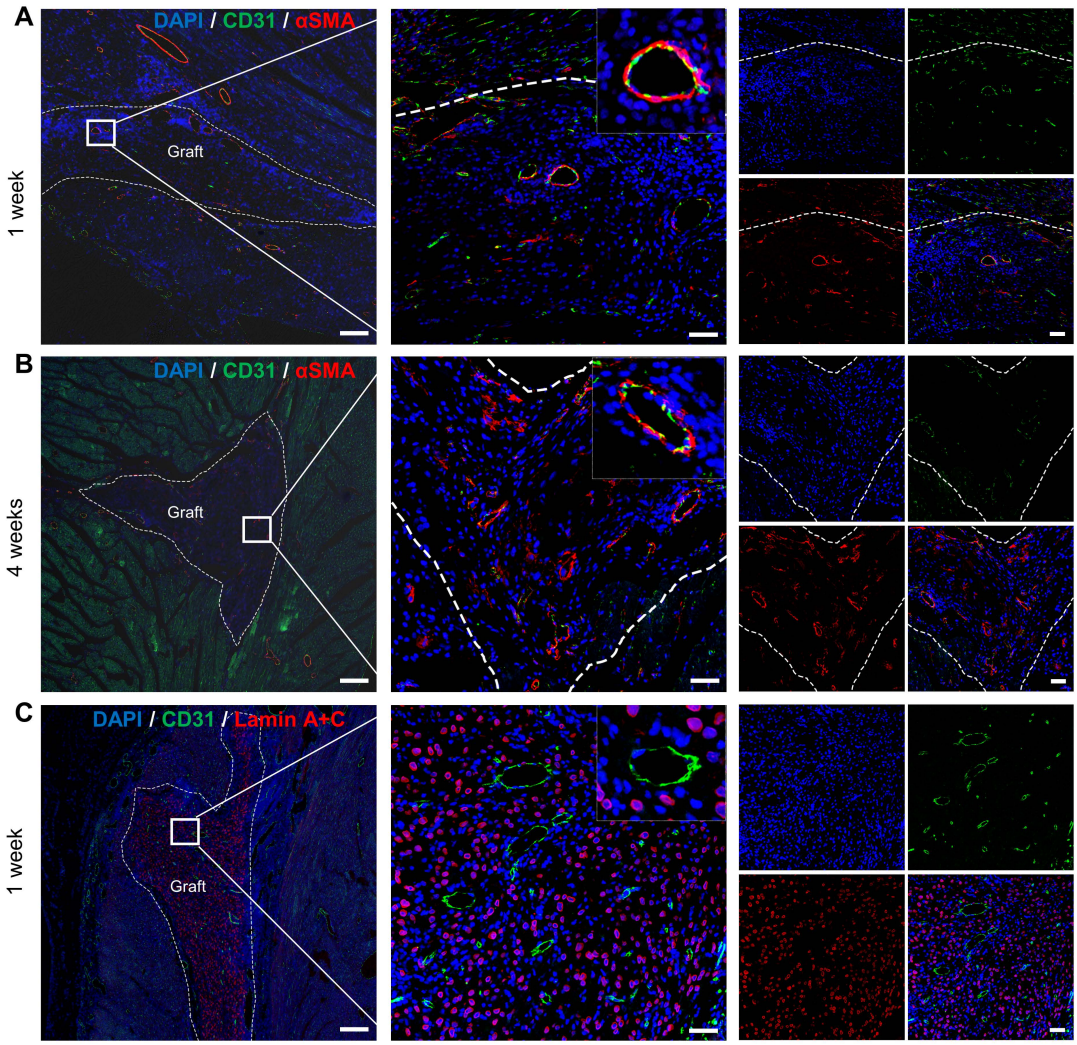

Figure S14. The vascularization of grafts following iPSC-CMs^{modVEGF} treatment

(A) Representative confocal pictures of α-SMA and CD31 expression in the myocardial grafts of iPSC-CMs^{modVEGF} at 1-week post-transplantation (scale bar: 200 μm), zoom in (scale bar: 50 μm). (B) Representative confocal pictures depicting α-SMA and CD31 expression in the engrafted region 4 weeks post-transplantation (scale bar: 200 μm, and enlarged pictures, scale bar: 50 μm). (C) Representative confocal pictures of the expression of Lamin A+C and CD31 in the myocardial grafts at 1-week post-transplantation of iPSC-CMs^{modVEGF} (scale bar: 200 μm, and enlarged pictures, scale bar: 50 μm).